

Slurry-phase ethylene polymerisation using group 4 *ansa*-bridged permethylindenyl complexes supported on polymethylaluminoxane

Jessica V. Lamb, Joseph C. Abell, Jack E. McLaren, Jean-Charles Buffet, Zoë R. Turner and Dermot O'Hare*

Chemistry Research Laboratory, Department of Chemistry, University of Oxford, 12 Mansfield Road, OX1 3TA
Oxford, UK. E-mail: dermot.ohare@chem.ox.ac.uk

Abstract

Five new group 4 *ansa*-bridged permethylindenyl complexes with either a dimethylsilane bridge or a tetramethyldisilane bridge have been synthesised and fully characterised. These complexes were supported on a hydrocarbon insoluble polymethylaluminoxane (sMAO) and the slurry-phase ethylene polymerisation performance was investigated. The highest activity was achieved using $\text{Me}_2\text{SB}(\text{Cp}^{\text{Me}}, \text{I}^*)\text{Zr}(\text{CH}_2\text{SiMe}_3)_2$ ($8042 \text{ kg}_{\text{PE}} \text{ mol}_{\text{Zr}}^{-1} \text{ h}^{-1} \text{ bar}^{-1}$ at 60°C) but a decrease in activity was observed with an increase in the length of the bridge. DSC analysis of the polymers revealed the production of HDPE with minimal branching and defects, while SEM showed the production of polymer particles with commercially desirable uniform, ‘popcorn’, morphology. GPC analysis showed the production of polyethylenes with $M_w < 570 \text{ kg mol}^{-1}$ at 80°C . In addition, $\text{Me}_2\text{SB}(\text{Cp}, \text{I}^*)\text{Zr}(\text{CH}_2\text{SiMe}_3)_2$ was immobilised on MAO modified layered double hydroxide (LDHMAO). The slurry-phase polymerisation activity of $\text{Me}_2\text{SB}(\text{Cp}, \text{I}^*)\text{Zr}(\text{CH}_2\text{SiMe}_3)_2$ on this support system was similar to the sMAO support, however the polymer morphology was much less uniform.

Keywords

Zirconocene, permethylindenyl, polymerisation, ethylene, layered double hydroxide

1 Introduction

Metallocene catalysts provide a multitude of possibilities for synthesising and controlling the structure and properties of polymers.[1-3] The single-site nature of metallocene catalysts leads to the formation of polymers with unimodal molecular weight distributions,[4] while *ansa*-bridges between the two cyclopentadienyl substituents can be employed to prevent ligand rotation and enforce complex rigidity.[5] Single atom silicon or carbon, and two atom carbon bridged metallocenes have been widely explored as catalysts for olefin polymerisation.[1, 5-

10] However, tetramethyldisilylene-bridged zirconocenes with the potential to combine the electronic and steric properties of both silyl and ethylene bridging groups have been far less studied; $^{\text{Me}_4}\text{DSB}(1\text{-C}_5\text{H}_3\text{-3-}^t\text{Bu})_2\text{ZrCl}_2$ ($^{\text{Me}_4}\text{DSB} = \text{Me}_4\text{Si}_2$) displays a solution-phase ethylene polymerisation activity of $2090 \text{ kg}_{\text{PE}} \text{ mol}_{\text{Zr}}^{-1} \text{ h}^{-1} \text{ bar}^{-1}$ at 30°C with methylaluminoxane (MAO) co-catalyst and 1 bar ethylene.[11]

Metallocene catalysts can be immobilised onto solid supports utilising the principles of surface organometallic chemistry,[12-19] in which the oxygen surface sites of the support act as anionic X-type ligands that covalently bond to the metal centre.[13-15, 20] The goal of immobilising α -olefin polymerisation catalysts is to preserve the advantages of homogeneous polymerisation, such as high activities and selectivities,[1, 21, 22] while improving polymer morphology *via* the templating effect of the solid support and reducing reactor fouling.[23-25] Many different types of solid support can be used for the immobilisation of metallocene catalysts, including highly Lewis acidic species such as MgCl_2 , $\text{SiO}_2\text{-Al}_2\text{O}_3$ and Al_2O_3 , and neutral or moderately Lewis acidic species such as SiO_2 and MgO . [13, 26, 27] Brønsted acidic species have also been shown to be efficient supports for the grafting of zirconocene catalyst precursors.[13, 28-30] These supports include highly Brønsted “super-acidic” sulfated metal oxides such as alumina, titania and zirconia.[28]

Solid polymethylaluminoxane (sMAO) is an insoluble form of oligomeric MAO that has recently been exploited as a solid support for metallocene pre-catalysts in slurry-phase olefin polymerisation.[7, 31-33] It is an oligomeric product of the incomplete hydrolysis of AlMe_3 (TMA) and consists of $(\text{AlMeO})_n$, where $n = 6\text{--}30$ monomer units.[34] The key advantage of sMAO as a metallocene support is that it can act as a bifunctional support and activator without further modification. We recently reported a range of unsymmetrical *ansa*-bridged permethylindenyl compounds of the type $^{\text{Me}_2}\text{SB}(\text{Cp}^{\text{R}}, \text{I}^*)\text{ZrX}_2$ ($\{(\eta^5\text{-C}_9\text{Me}_6)\text{Me}_2\text{Si}(\eta^5\text{-C}_5\text{H}_3\text{R})\}\text{ZrX}_2$; $\text{R} = \text{H}, \text{Me}$ and ^nBu ; $\text{X} = \text{Cl}, \text{Br}, \text{Me}$ and CH_2Ph) and $^{\text{R}_2}\text{SB}(^t\text{Bu}_2\text{Flu}, \text{I}^*)\text{ZrX}_2$ ($\{(\eta^5\text{-C}_9\text{Me}_6)\text{R}_2\text{Si}(\eta^5\text{-2,9-}^t\text{Bu-C}_{13}\text{H}_6)\}\text{ZrX}_2$, $\{(\eta^5\text{-I}^*)\text{R}_2\text{Si}(\eta^5\text{-2,9-}^t\text{Bu-Flu})\}\text{ZrX}_2$; $\text{R} = \text{Me}, \text{Et}$ and $\text{X} = \text{Cl}$ and Br) for slurry-phase ethylene polymerisation (Chart 1).[7, 35, 36] When immobilised on sMAO the species showed activities up to 83% higher than an industrial standard, $(\text{Cp}^{^n\text{Bu}})_2\text{ZrCl}_2$, under the same polymerisation conditions.[35]

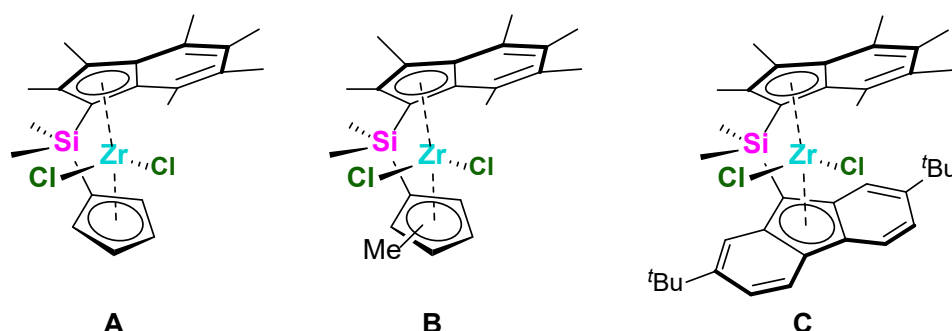


Chart 1. Example of previously reported group 4 permethylindenyl complexes $\text{Me}_2\text{SB}(\text{Cp},\text{I}^*)\text{ZrCl}_2$ (A), [36] $\text{Me}_2\text{SB}(\text{Cp}^{\text{Me}},\text{I}^*)\text{ZrCl}_2$ (B) [36] and $\text{Me}_2\text{SB}(\text{}^t\text{Bu}_2\text{Flu},\text{I}^*)\text{ZrCl}_2$ (C). [7]

2 Results and Discussion

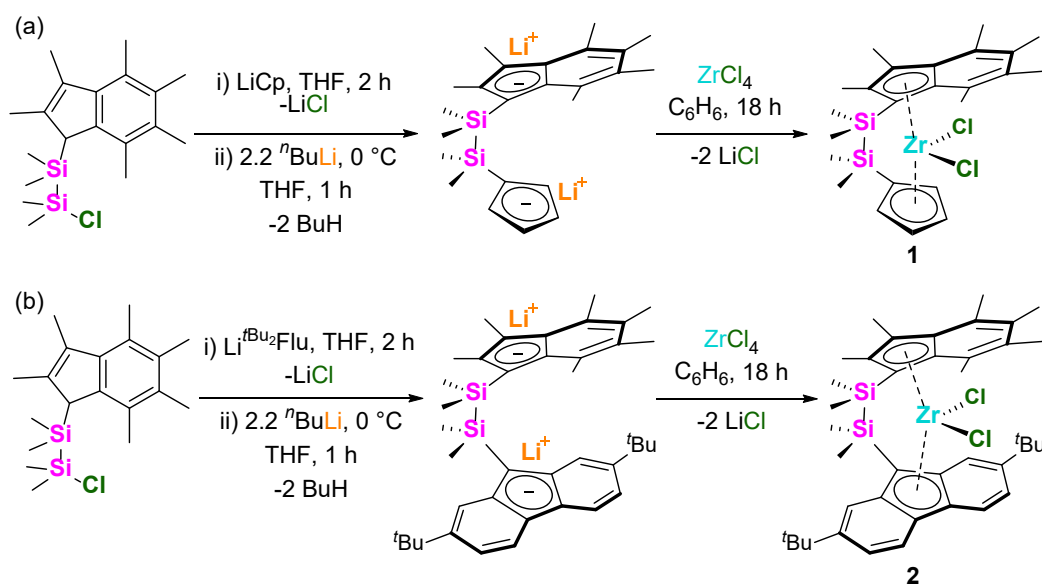
2.1 Synthesis of $\text{Me}_4\text{DSB}(\text{Cp},\text{I}^*)\text{Li}_2$ and $\text{Me}_4\text{DSB}(\text{}^t\text{Bu}_2\text{Flu},\text{I}^*)\text{Li}_2$ ligands

$\text{Ind}^*(\text{SiMe}_2)_2\text{Cl}$ was synthesised in an analogous fashion to previously reported $\text{Ind}^*\text{SiMe}_2\text{Cl}$; [36] hexamethylindene (Ind^{H}) was deprotonated with 1.1 equivalents of *n*-butyllithium and the product added to 3.0 equivalents of $\text{Me}_4\text{Si}_2\text{Cl}_2$. Following workup, $\text{Ind}^*(\text{SiMe}_2)_2\text{Cl}$ was isolated as a pale yellow solid in 70% yield. The ^1H NMR spectrum shows four singlets between -0.21 and 0.36 ppm corresponding to the protons of the silyl bridge methyl groups, six singlets between 2.10 and 2.49 ppm corresponding to the methyl groups of the permethylindenyl ligand and a resonance at 3.55 ppm corresponding to the allylic proton of the indenyl ring (Figure S1).

Analogous to the synthesis of $\text{Me}_2\text{SB}(\text{Cp},\text{I}^*)\text{Li}_2$, [36] dilithium salts $\text{Me}_4\text{DSB}(\text{Cp},\text{I}^*)\text{Li}_2$ ($\{(\eta^5\text{-C}_9\text{Me}_6)\text{Me}_4\text{Si}_2(\eta^5\text{-C}_5\text{H}_5)\}\text{Li}_2$) and $\text{Me}_4\text{DSB}(\text{}^t\text{Bu}_2\text{Flu},\text{I}^*)\text{Li}_2$ were prepared by the reaction of equimolar quantities of $\text{Ind}^*(\text{SiMe}_2)_2\text{Cl}$ and LiCp or $\text{Li}(\text{}^t\text{Bu}_2\text{Flu})$ respectively, followed by deprotonation with two equivalents of *n*BuLi (Scheme 1). Following work up, $\text{Me}_4\text{DSB}(\text{Cp},\text{I}^*)\text{Li}_2$ and $\text{Me}_4\text{DSB}(\text{}^t\text{Bu}_2\text{Flu},\text{I}^*)\text{Li}_2 \cdot (\text{Et}_2\text{O})_{1.5}$ were obtained in 78 and 19% yield respectively. The ^1H NMR spectra show six singlets between 2.24 and 3.06 ppm corresponding to the methyl groups on the indenyl ring and two singlets at 0.83 and 1.28 ppm corresponding to the methyl groups on the disilylene bridging moiety (Figures S3 and S5). The ^1H NMR spectrum of $\text{Me}_4\text{DSB}(\text{Cp},\text{I}^*)\text{Li}_2$ also shows multiplets at 6.27 and 6.56 ppm corresponding to the protons on the cyclopentadienyl ring, while $\text{Me}_4\text{DSB}(\text{}^t\text{Bu}_2\text{Flu},\text{I}^*)\text{Li}_2$ shows a singlet at 1.64 ppm and three resonances at 7.12 , 8.47 and 8.50 ppm corresponding to the *tert*-butyl and aromatic protons of the $\text{}^t\text{Bu}_2\text{Flu}$ ligand.

2.2 Synthesis of $\text{Me}_4\text{DSB}(\text{Cp},\text{I}^*)\text{ZrCl}_2$ (**1**) and $\text{Me}_4\text{DSB}(\text{}^t\text{Bu}_2\text{Flu},\text{I}^*)\text{ZrCl}_2$ (**2**)

Equimolar mixtures of dilithium salts $\text{Me}_4\text{DSB}(\text{Cp},\text{I}^*)\text{Li}_2$ or $\text{Me}_4\text{DSB}(\text{}^t\text{Bu}_2\text{Flu},\text{I}^*)\text{Li}_2(\text{Et}_2\text{O})_{1.5}$ and ZrCl_4 were stirred in benzene for 16 hours at room temperature (Scheme 1). Following work up, $\text{Me}_4\text{DSB}(\text{Cp},\text{I}^*)\text{ZrCl}_2$ (**1**) and $\text{Me}_4\text{DSB}(\text{}^t\text{Bu}_2\text{Flu},\text{I}^*)\text{ZrCl}_2$ (**2**) were isolated as orange solids in 13 and 52% yield respectively. The ^1H NMR spectra of **1** and **2** show six singlets of equal intensity between 1.98 and 2.84 ppm corresponding to the methyl groups of the indenyl ring and four singlets between 0.35 and 0.86 ppm corresponding to the methyl groups of the disilyl bridge (Figures S7 and S9). The ^1H NMR spectrum of **1** also shows multiplet resonances corresponding to the protons on the cyclopentadienyl ring between 5.67 and 6.84 ppm, while **2** shows the *tert*-butyl groups of the fluorenyl ligand as singlets at 1.32 and 1.40 ppm and the three aromatic proton environments of the fluorenyl ligand as doublets of doublets at 7.40 and 7.59 ppm, singlets at 7.69 and 7.62 ppm and doublets at 7.70 and 7.86 ppm.



Scheme 1. Synthesis of $\text{Me}_4\text{DSB}(\text{Cp},\text{I}^*)\text{ZrCl}_2$ (**1**) and $\text{Me}_4\text{DSB}(\text{}^t\text{Bu}_2\text{Flu},\text{I}^*)\text{ZrCl}_2$ (**2**).

Crystals of **2** suitable for a single crystal X-ray diffraction study were grown from pentane at $-34\text{ }^\circ\text{C}$. The solid-state molecular structure is depicted in Figure 1, with selected bond lengths and angles presented in Table 1. Complex **2** displays a similar $\text{Zr-Flu}_{\text{cent}}$ distance to the corresponding mono-silyl bridged species $\text{Me}_2\text{SB}(\text{}^t\text{Bu}_2\text{Flu},\text{I}^*)\text{ZrCl}_2$ (2.3144 and 2.300 Å respectively),[7] however possesses a slightly longer $\text{Zr-Ind}_{\text{cent}}$ distance (2.2540 and 2.227 Å respectively) due to the longer length of the bridge. Complex **2** also displays a longer $\text{Zr-Ind}_{\text{cent}}$ distance than *rac*-EBI* ZrCl_2 and *meso*-EBI* ZrCl_2 (average $\text{Zr-Ind}_{\text{cent}}$ of 2.240 and 2.246 Å respectively)[8] and longer Zr-centroid distances than *meso*- $\text{Me}_4\text{DSB}(1\text{-C}_5\text{H}_3\text{-3-}^t\text{Bu})_2\text{ZrCl}_2$ and

rac-^{Me}₄EB(1-C₅H₃-3-^tBu)₂ZrCl₂ (average Zr-Cp^R_{cent} of 2.238 and 2.227 Å).[11, 37] **2** shows a larger angle about the metal centre (δ) and smaller ring tilt angle (α) than ^{Me}₂SB(^tBu₂Flu,I*)ZrCl₂ (δ = 139.70° and 131.0°; α = 54.91° and 62.04°), implying that the two atom disilyl bridge causes a lesser degree of ring tilt and a less open and less available metal centre than the one atom silyl bridge. The α and δ angles of **2** are larger than the values reported for *meso*-^{Me}₄DSB(3-SiMe₃-Ind)₂ZrCl₂ (α = 47.8° and δ = 134.6°) suggesting that the unsymmetrical system causes a larger degree of ring tilt.[38] The C-Si-Si angles of the bridge for **2** (103.05° and 102.10°) are comparable to those recorded for *meso*-^{Me}₄DSB(3-SiMe₃-Ind)₂ZrCl₂ (103.30° and 102.69°).[38] However, the C-Si-Si angles for **2** are larger than the C-Si-C angle recorded for ^{Me}₂SB(^tBu₂Flu,I*)ZrCl₂ (95.61°), implying a smaller degree of strain in the bridge.[7]

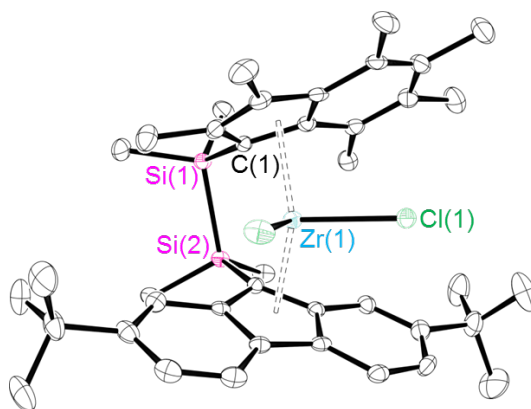


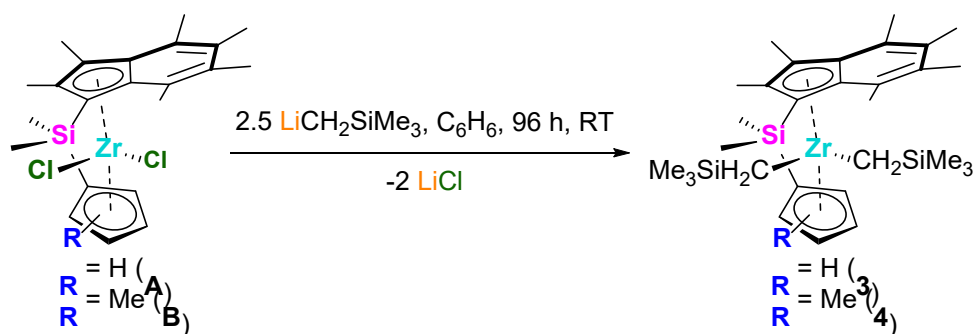
Figure 1. Solid-state molecular structure of ^{Me}₄DSB(^tBu₂Flu,I*)ZrCl₂ (**2**). H atoms omitted for clarity. Thermal ellipsoids drawn at 30% probability.

Table 1. Selected bond lengths (Å) and angles (°) for **2**, **A** and **5**.

	Complex	Zr(1)-Cp ^R _{cent}	Zr(1)-Ind _{cent}	α	δ
2	^{Me} ₄ DSB(^t Bu ₂ Flu, I*)ZrCl ₂	2.3347(1) ^a	2.2714(1)	54.91	139.70
	^{Me} ₂ SB(^t Bu ₂ Flu, I*)ZrCl ₂ [7]	2.300 ^a	2.227	62.04	131.0
	<i>meso</i> - ^{Me} ₄ DSB(3-SiMe ₃ -Ind) ₂ ZrCl ₂ [38]	-	2.261 ^b	47.8	134.64
	<i>rac</i> -EBI*ZrCl ₂ [8]	-	2.240 ^b	57.2	129.4
	<i>meso</i> -EBI*ZrCl ₂ [8]	-	2.246 ^b	56.9	128.7
A	^{Me} ₂ SB(Cp, I*)ZrCl ₂ [35]	2.2076(1)	2.2244(1)	60.19	126.37
5	^{Me} ₂ SB(Cp, I*)ZrCl(O-2,6- ⁱ Pr-C ₆ H ₃)	2.2070(1)	2.2462(1)	59.62	125.29
	^{Me} ₂ SB(Cp, I*)ZrCl(O-2,6-Me-C ₆ H ₃)[36]	2.2201(1)	2.2504(1)	60.88	126.90

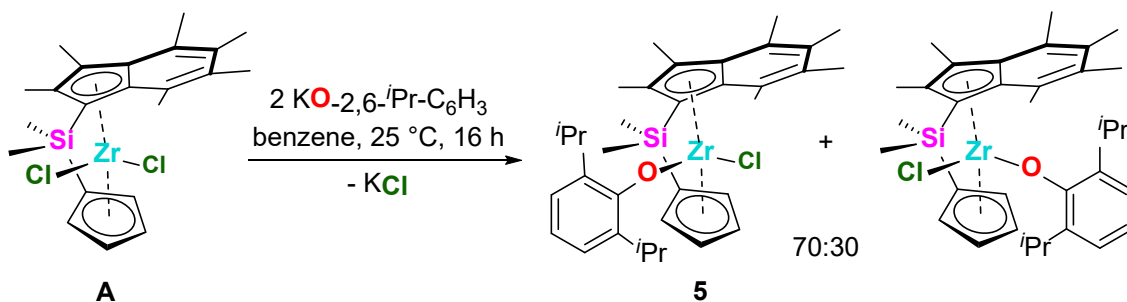
(a) Zr-Flu_{cent} distance and (b) average Zr-Ind_{cent} distance.**2.3 Synthesis of ^{Me}₂SB(Cp^R, I*)ZrR'₂ (R = H and Me; R' = CH₂SiMe₃ and O-2,6-ⁱPr-C₆H₃)**

^{Me}₂SB(Cp, I*)ZrCl₂ (**A**) and ^{Me}₂SB(Cp^{Me}, I*)ZrCl₂ (**B**) were synthesised according to a literature procedure; [36] as reported, **B** was obtained as a 60:40 mixtures of two isomers with the methyl group at the *gamma* positions of the Cp ring. The reaction of **A** and **B** with 2.5 equivalents of LiCH₂SiMe₃ afforded ^{Me}₂SB(Cp, I*)Zr(CH₂SiMe₃)₂ (**3**) and ^{Me}₂SB(Cp^{Me}, I*)Zr(CH₂SiMe₃)₂ (**4**) as yellow solids in 12 and 53% yield respectively (Equation 1). The ¹H NMR spectra of **3** and **4** showed cyclopentadienyl, permethylindenyl methyl and silyl bridge methyl resonances at 4.94–6.90, 1.83–2.90 and 0.62–0.69 ppm respectively (Figures S11 and S13). The ¹H NMR spectra also showed singlet resonances at –0.02–0.21 ppm and doublet resonances at –2.49–0.69 ppm corresponding to the methyl groups and diastereotopic CH₂ protons of the neosilyl ligand respectively. The ¹H NMR spectrum of **4** confirmed that the 60:40 mixture of isomers in the parent dichloride complex, where the methyl substituent lies in the γ -position of the cyclopentadienyl ring furthest and nearest to the permethylindenyl group respectively, is maintained in the product.



Equation 1. Synthesis of $\text{Me}_2\text{SB}(\text{Cp},\text{I}^*)\text{Zr}(\text{CH}_2\text{SiMe}_3)_2$ (**3**) and $\text{Me}_2\text{SB}(\text{Cp}^{\text{Me}},\text{I}^*)\text{Zr}(\text{CH}_2\text{SiMe}_3)_2$ (**4**)

The reaction of **A** with two equivalents $\text{KO}-2,6\text{-}i\text{Pr}-\text{C}_6\text{H}_3$ yielded $\text{Me}_2\text{SB}(\text{Cp},\text{I}^*)\text{ZrCl}(\text{O}-2,6\text{-}i\text{Pr}-\text{C}_6\text{H}_3)$ as a mixture of the two mono-substituted isomers in a 70:30 ratio, where the aryloxy group is positioned away from and underneath the I^* ligand respectively. $\text{Me}_2\text{SB}(\text{Cp},\text{I}^*)\text{ZrCl}(\text{O}-2,6\text{-}i\text{Pr}-\text{C}_6\text{H}_3)$ (**5**) was obtained as a single isomer from a pentane solution at $-34\text{ }^\circ\text{C}$ in 14% yield, determined by ROESY NMR spectroscopy to have the aryloxy group positioned away from the I^* ligand (Equation 2). In addition to the diagnostic cyclopentadienyl, permethylindenyl methyl and silyl bridge methyl resonances at 5.71–6.40, 5.15–2.46 and 0.66–0.77 ppm, **5** also shows resonances at 6.99–7.14, 3.61–3.07 and 1.30 ppm corresponding to the aromatic, *iso*-propyl methyl and *iso*-propyl CH protons respectively (Figure S15).



Equation 2. Synthesis of $\text{Me}_2\text{SB}(\text{Cp},\text{I}^*)\text{ZrCl}(\text{O}-2,6\text{-}i\text{Pr}-\text{C}_6\text{H}_3)$ (**5**).

Yellow crystals of **5** suitable for a single crystal X-ray diffraction study were obtained from a saturated pentane solution at $-34\text{ }^\circ\text{C}$. The solid-state molecular structure is depicted in Figure 2, with selected bond lengths and angles presented in Table 1. The solid-state structure confirms isolation of the isomer with the aryloxy group positioned away from the I^* ligand. This is in contrast to previously reported $\text{Me}_2\text{SB}(\text{Cp},\text{I}^*)\text{ZrCl}(\text{O}-2,6\text{-Me}-\text{C}_6\text{H}_3)$ where the isomer with the aryloxy group positioned below the I^* ring is favoured. The change in positioning the aryloxy ligand when moving from the methyl to the *iso*-propyl substituted aryloxy

moiety can be rationalised due to the sterics of the systems; the bulkier *iso*-propyl group is less likely to be positioned in the more sterically inaccessible position below the permethylindenyl ring.

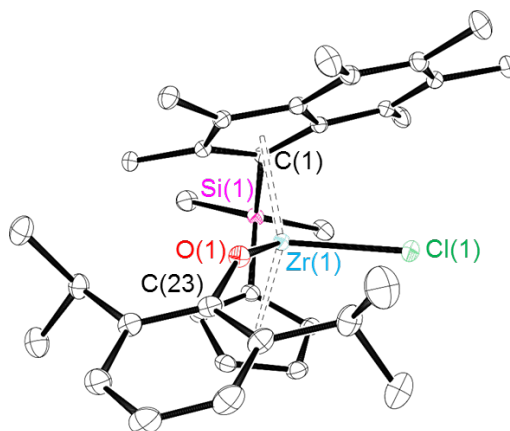


Figure 2. Solid-state molecular structure of $\text{Me}_2\text{SB}(\text{Cp}, \text{I}^*)\text{ZrCl}(\text{O}-2,6\text{-}i\text{Pr}-\text{C}_6\text{H}_3)$ (**5**). H atoms omitted for clarity. Thermal ellipsoids drawn at 30% probability.

Complex **5** shows Zr-O distances comparable to the values reported for $\text{Cp}_2\text{ZrCl}(\text{O}-2,6\text{-}i\text{Pr}-\text{C}_6\text{H}_3)$ and $\text{Me}_2\text{SB}(\text{Cp}, \text{I}^*)\text{ZrCl}(\text{O}-2,6\text{-Me}-\text{C}_6\text{H}_3)$; Zr-O = 1.9873(11), 1.97(1) and 1.9628(12) Å respectively).[36, 39] The Zr-O bond lengths reported for **5** are significantly shorter than the sum of the covalent radii of zirconium and oxygen (1.75 and 0.66 Å respectively), indicating that there is partial ionic character to the Zr-O bond.[40] Complex **5** displays a smaller Zr-O-C angle than $\text{Me}_2\text{SB}(\text{Cp}, \text{I}^*)\text{ZrCl}(\text{O}-2,6\text{-Me}-\text{C}_6\text{H}_3)$ (148.31(11)° and 173.09(12)° respectively), which suggests a lesser degree of π -orbital overlap between Zr and O.[36] The Zr-Cp^R_{cent} and Zr-Ind_{cent} distances of **5** are comparable to $\text{Me}_2\text{SB}(\text{Cp}, \text{I}^*)\text{ZrCl}(\text{O}-2,6\text{-Me}-\text{C}_6\text{H}_3)$ and the parent dichloride complex **A** (Zr-Cp^R_{cent} = 2.2070(1), 2.2201(1) and 2.2076(1) Å; Zr-Ind_{cent} = 2.2462(1), 2.2504(1) and 2.2244(1) Å respectively), while α and δ are relatively unaffected by ligand substitution from chloride to aryloxy (α = 59.62° and 60.19°; δ = 125.29° and 126.37° for **5** and **A** respectively).[36]

2.3 Polymerisation studies using sMAO

Complexes **1-5** were immobilised onto solid polymethylaluminoxane (sMAO), according to a literature procedure,[9] with an initial aluminium (in sMAO) to zirconium ($[\text{Al}_{\text{sMAO}}]_0/[\text{Zr}]_0$) loading of 200 (Tables S3–S7). Characterisation of three sMAO supported complexes (**1**_{sMAO}, **2**_{sMAO} and **3**_{sMAO}) was achieved using solid-state NMR spectroscopy (SSNMR) (Figures S17–S25). The ¹³C CP/MAS SSNMR spectra show a dominant resonance at approximately –8 ppm corresponding to the methyl groups present within the sMAO support. The spectra also show

resonances between 15 and 40 ppm corresponding to the methyl groups of the silyl bridge moiety and indenyl rings, in addition to the *t*-butyl groups on the fluorenyl ring for **2_{sMAO}** (Figure S20) and the methyl groups of the neosilyl ligand for **3_{sMAO}** (Figure S23), and resonances between 120 and 140 ppm corresponding to the carbon atoms of the arene rings in all three complexes. The ²⁹Si CP/MAS SSNMR spectra of **1_{sMAO}** and **2_{sMAO}** show a single broad resonance with maxima at -12.9 and -5.2 ppm respectively; separate environments for the two silicon atoms of the bridge cannot be identified (Figures S18 and S21). The ²⁹Si CP/MAS SSNMR spectrum of **3_{sMAO}** shows two resonances at -11.76 and 0.55 ppm corresponding to the silicon atoms of the neosilyl ligand and bridge respectively (Figure S24). The ²⁷Al DP/MAS SSNMR spectra for all three complexes showed a series of broad resonances between -245 and 350 ppm due to the quadrupolar aluminium nucleus (*I* = 5/2).

In order to determine the ideal scavenger for polymerisation, **A** was supported on sMAO (**A_{sMAO}**) with an initial aluminium to metal ($[Al]_{sMAO} / [Zr]_0$) loading of 200. Alkyl aluminium species are often added during slurry-phase polymerisation with metallocene catalysts immobilised on activated supports to scavenge impurities such as trace water and oxygen. However, they can also be used to control catalyst activity and influence polymer properties.[41-43] Slurry-phase ethylene polymerisation reactions were conducted in 150 mL ampoules with 50 mL hexane, 10 mg pre-catalyst and 2 bar ethylene at 80 °C for 30 minutes using four different scavengers (trimethylaluminium, TMA; triethylaluminium, TEA; triisobutylaluminium, TiBA; methylaluminoxane, MAO) with an initial scavenger to zirconium ($[Al]_{scav} / [Zr]_0$) ratio of 1000.

It is noted that utilising MAO as the scavenger resulted in the formation of very aggregated polymer particles, likely caused by leaching of the metallocene into solution,[44] which caused stirring to cease after approximately 15 minutes. The highest polymerisation activity was recorded with TiBA, followed by TEA, MAO and TMA; activities of 5144, 4649, 3879 and 3013 kg_{PE} mol_{Zr}⁻¹ h⁻¹ bar⁻¹ respectively (Figure 3 and Table S3). It is proposed that a decrease in activity on moving from TiBA to TEA scavengers may be due to formation of more stable heterobimetallic species such as $[Cp_2M(\mu-CH_2R')(\mu-R)AlR_2]^+$, where R is an alkyl group from the aluminium species.[45-47] It has been reported that the stability of μ -alkyl complexes decrease with increasing bulk of the alkyl group, implying that the lower activity observed with TEA and TMA scavengers compared to TiBA is due to the higher stability of the heterobimetallic formed.

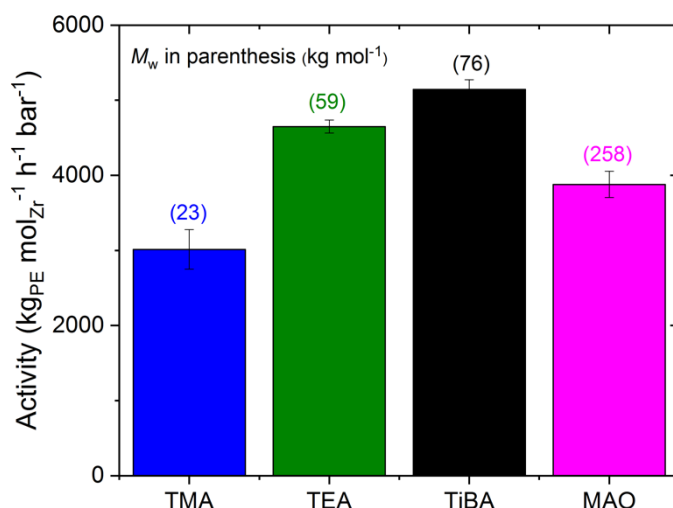


Figure 3. Slurry-phase ethylene polymerisation activity using solid MAO supported $\text{Me}_2\text{SB}(\text{Cp}, \text{I}^*)\text{ZrCl}_2$ (A_{sMAO}) with TMA (blue), TEA (green), TiBA (black) and MAO (pink) scavengers. Polymerisation conditions: $[\text{Al}_{\text{sMAO}}]_0/[\text{Zr}]_0 = 200$, scavenger ($[\text{Al}_{\text{scav}}]_0/[\text{Zr}]_0 = 1000$), ethylene (2 bar), pre-catalyst (10 mg), hexane (50 mL), 80 °C and 30 minutes. Molecular weights (M_w , kg mol⁻¹ given in parentheses).

The polyethylenes produced using A_{sMAO} with TMA, TEA, TiBA and MAO scavengers were analysed by gel permeation chromatography (GPC) (Figures 3 and 4a). The lower molecular weights (M_w) of the polymers produced using TMA and TEA compared to TiBA and MAO can be attributed to the increase in steric bulk of TiBA and MAO, which may slow the rate of chain transfer to aluminium ($M_w = 23, 59, 76$ and 258 kg mol⁻¹). [48, 49] Differential scanning calorimetry (DSC) analysis of the polymers revealed melting temperatures (T_m) of 132–134 °C and crystallisation temperatures (T_c) of 119–122 °C (Figure 4b and Table S10), demonstrating the production of high-density polyethylenes (HDPE) with minimal defects and branching. [50, 51] The enthalpy of melting (ΔH_m) and cooling (ΔH_c) were calculated from the DSC plots to be in the range 138–220 J g⁻¹ and 143–256 J g⁻¹ respectively. The polymers produced using TMA, TEA and TiBA as scavengers showed a higher crystallinity than those produced using MAO; 69, 87, 71 and 49% respectively. Crystallinity is usually fairly high for HDPE as the lack of branching allows the chains to pack closely together, which leads to a higher degree of long-range order in the material. [52] The lower crystallinity of the polymers produced from MAO may be due the inhomogeneous polymer morphology observed as polymerisation proceeded. Crystallinity can also be affected by polymer molecular weights; higher molecular

weight polymers typically have a higher degree of chain entanglement, which can lead to a lower crystallinity when relaxing from the melt.[53, 54]

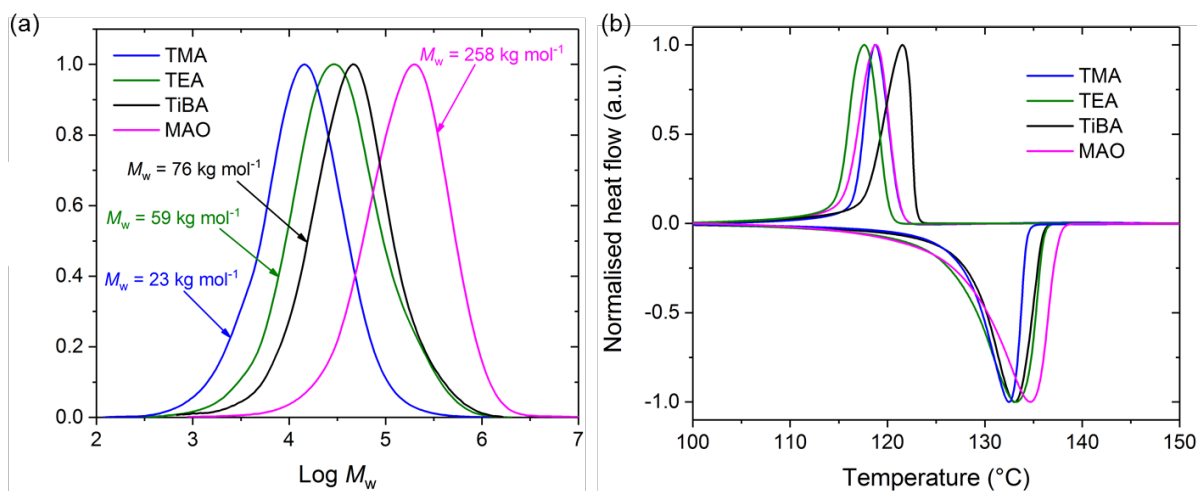


Figure 4. (a) Molecular weights distribution and (b) DSC plot showing the first cooling cycle and second heating cycle for the polyethylenes produced using sMAO supported $\text{Me}_2\text{SB}(\text{Cp}, \text{I}^*)\text{ZrCl}_2$ (A_{sMAO}) with TMA (blue), TEA (green), TiBA (black) and MAO (pink) scavenger. Normalised for clarity. Polymerisation conditions: $[\text{Al}_{\text{sMAO}}]_0/[\text{Zr}]_0 = 200$, scavenger ($[\text{Al}_{\text{scav}}]_0/[\text{Zr}]_0 = 1000$), ethylene (2 bar), pre-catalyst (10 mg), hexane (50 mL), 80 °C and 30 minutes.

Following on from this study, the slurry-phase polymerisation of ethylene using **1-5** supported on sMAO was investigated. Polymerisations were conducted in 150 mL ampoules with 150 mg TiBA ($[\text{Al}_{\text{scav}}]_0/[\text{Zr}]_0 = 1000$), 50 mL hexane, 10 mg pre-catalyst and 2 bar ethylene for 30 minutes between 50 and 90 °C. Figure 5 shows that **1**_{sMAO}, **2**_{sMAO} and **5**_{sMAO} display significantly lower slurry-phase ethylene polymerisation activities than **3**_{sMAO} and **4**_{sMAO}; 573, 355, 549, 4301 and 3564 $\text{kg}_{\text{PE}} \text{mol}_{\text{Zr}}^{-1} \text{h}^{-1} \text{bar}^{-1}$ respectively at 80 °C. The disilyl bridged species **1**_{sMAO} and **2**_{sMAO} also display much lower polymerisation activities than the monosilyl bridges analogues (activities of 5144 and 6013 $\text{kg}_{\text{PE}} \text{mol}_{\text{Zr}}^{-1} \text{h}^{-1} \text{bar}^{-1}$ for sMAO- $\text{Me}_2\text{SB}(\text{Cp}, \text{I}^*)\text{ZrCl}_2$ and sMAO- $\text{Me}_2\text{SB}(\text{tBu}_2\text{Flu}, \text{I}^*)\text{ZrCl}_2$ respectively at 80 °C).[7, 35] The decreased activity is likely due to the increased flexibility of the disilyl bridge.[6] For **2**_{sMAO}, the lower polymerisation activity may also be a consequence of the decreased size of the coordination site when compared to $\text{Me}_2\text{SB}(\text{tBu}_2\text{Flu}, \text{I}^*)\text{ZrCl}_2$ ($\delta = 139.7^\circ$ and 131.0° respectively),[7] which may reduce the accessibility of the metal centre to ethylene monomers.

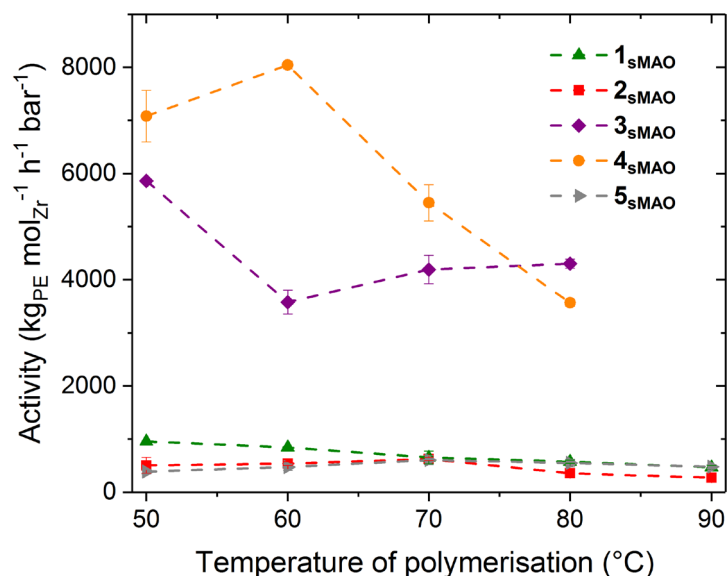


Figure 5. Slurry-phase ethylene polymerisation activity as a function of temperature of polymerisation using sMAO supported $\text{Me}_4\text{DSB}(\text{Cp}, \text{I}^*)\text{ZrCl}_2$ (**1**_{sMAO}; green triangle), $\text{Me}_4\text{DSB}(\text{tBu}_2\text{Flu}, \text{I}^*)\text{ZrCl}_2$ (**2**_{sMAO}; red square), $\text{Me}_2\text{SB}(\text{Cp}, \text{I}^*)\text{Zr}(\text{CH}_2\text{SiMe}_3)_2$ (**3**_{sMAO}; purple diamond), $\text{Me}_2\text{SB}(\text{Cp}^{\text{Me}}, \text{I}^*)\text{Zr}(\text{CH}_2\text{SiMe}_3)_2$ (**4**_{sMAO}; orange circle) and $\text{Me}_2\text{SB}(\text{Cp}, \text{I}^*)\text{ZrCl}(\text{O}-2,6\text{-}i\text{Pr}-\text{C}_6\text{H}_3)$ (**5**_{sMAO}; grey right triangle). Polymerisation conditions: $[\text{Al}_{\text{sMAO}}]_0/[\text{Zr}]_0 = 200$, TiBA (150 mg), ethylene (2 bar), pre-catalyst (10 mg), hexane (50 mL) and 30 minutes.

The addition of an aryloxy group significantly reduces the polymerisation activity of **5**_{sMAO} compared to parent dichloride complex **A**_{sMAO} (activities of 549 and 5144 $\text{kgPE molZr}^{-1} \text{ h}^{-1} \text{ bar}^{-1}$ respectively at 80 °C). This is opposite to the effect seen by Firth *et al.*, where the solution-phase polymerisation of ethylene with $\text{Cp}_2\text{ZrCl}(\text{O}-2,6\text{-}i\text{Pr}-\text{C}_6\text{H}_3)$ showed an 11% increase in activity compared to the parent dichloride complex Cp_2ZrCl_2 (1 bar ethylene at room temperature).[39] Conversely, Repo *et al.* reported that the solution-phase polymerisation of ethylene with $\text{Cp}_2\text{ZrCl}(\text{O}-2,6\text{-}i\text{Pr}-\text{C}_6\text{H}_3)$ with 2 bar ethylene at 30 °C gave a slightly lower polymerisation activity than Cp_2ZrCl_2 (995 and 1100 $\text{kgPE molZr}^{-1} \text{ h}^{-1} \text{ bar}^{-1}$ respectively).[55] In order to further understand the mechanism of polymerisation, Firth *et al.* demonstrated that the reaction of $\text{Cp}_2\text{ZrCl}(\text{O}-2,6\text{-}i\text{Pr}-\text{C}_6\text{H}_3)$ with two equivalents of TMA resulted in the formation of Cp_2ZrMe_2 (via $\text{Cp}_2\text{ZrMe}(\text{O}-2,6\text{-}i\text{Pr}-\text{C}_6\text{H}_3)$) and aluminium by-product $[\text{AlMe}_2(\text{O}-2,6\text{-}i\text{Pr}-\text{C}_6\text{H}_3)]_n$,[39] highlighting that polymerisation activity is at least partially dependent on the efficiency of X ligand abstraction by the co-catalyst. It is postulated that the leaving group becomes bound to the solid support during immobilisation.[56] Therefore, the

bulky aryloxy group could influence polymerisation activity by altering the second order sphere of coordination of the catalyst,[57] potentially weakening the interaction between the inner-sphere ion pair (composed of the cationic catalyst and anionic counterion)[57] and reducing the barriers to insertion.[58, 59]

3_sMAO shows a fairly constant activity across the temperature range (between 5862 and 4302 kg_{PE} mol_{Zr}⁻¹ h⁻¹ bar⁻¹), but a lower polymerisation activity than the dichloride analogue **A_sMAO** (activities of 5862 and 6794 kg_{PE} mol_{Zr}⁻¹ h⁻¹ bar⁻¹ at 50 °C respectively). In contrast, **4_sMAO** shows a sharp decrease in polymerisation activity above 60 °C, indicating a lack of thermal stability, and a higher polymerisation activity than the dichloride analogue **B_sMAO** before decomposition (activities of 8042 and 4223 kg_{PE} mol_{Zr}⁻¹ h⁻¹ bar⁻¹ respectively at 60 °C). When compared to the benzyl analogues, **3_sMAO** shows a lower polymerisation activity than Me₂SB(Cp,I*)Zr(CH₂Ph)₂ across the temperature range while **4_sMAO** shows a higher activity than Me₂SB(Cp^{Me},I*)Zr(CH₂Ph)₂ below 70 °C (activities of 6265 and 6729 kg_{PE} mol_{Zr}⁻¹ h⁻¹ bar⁻¹ respectively at 60 °C).[35]

1_sMAO, **2_sMAO** and **5_sMAO** show significantly lower ethylene polymerisation activities across the temperature range than industrial standard sMAO-(Cp^{nBu})₂ZrCl₂ under the same conditions (573, 355, 549 and 3459 kg_{PE} mol_{Zr}⁻¹ h⁻¹ bar⁻¹ respectively at 80 °C). **3_sMAO** shows a higher activity than sMAO-(Cp^{nBu})₂ZrCl₂ at all temperatures except 60 °C (5862 and 4367 kg_{PE} mol_{Zr}⁻¹ h⁻¹ bar⁻¹ respectively at 50 °C), while **4_sMAO** shows a higher activity than sMAO-(Cp^{nBu})₂ZrCl₂ below 70 °C (8042 and 4641 kg_{PE} mol_{Zr}⁻¹ h⁻¹ bar⁻¹ respectively at 60 °C).

The polyethylenes produced using **1_sMAO**, **2_sMAO**, **3_sMAO** and **5_sMAO** were analysed by GPC (Figure 6). *M_w* was observed to decrease with increasing polymerisation temperature, attributed to faster chain transfer reactions at higher temperatures,[60] and an increase in the rate of termination relative to propagation; at elevated temperatures, the system has more energy to overcome the higher activation barrier of termination.[61] **2_sMAO** produced polymers with the highest molecular weights, followed by **1_sMAO**, **3_sMAO** and **5_sMAO**; *M_w* = 567, 289, 196 and 160 kg mol⁻¹ at 80 °C. This implies that the longer the silyl bridging moiety, the higher the molecular weight of the resulting polyethylenes. **1_sMAO** and **2_sMAO** produced polymers with molecular weights approximately 3.5 and 1.3 times larger than the corresponding one atom silyl bridged species sMAO-Me₂SB(Cp,I*)ZrCl₂ and sMAO-Me₂SB(^tBu₂Flu,I*)ZrCl₂. [7, 35] The polymers also displayed wide molecular weight distributions (*M_w*/*M_n* = 6.7–8.1 and 8.4–17.9 for **1_sMAO** and **2_sMAO** respectively) implying that a variety of surface sites may exist. **3_sMAO** and **5_sMAO** produced polymers with molecular weights lower than **1_sMAO** and **2_sMAO**; however, *M_w*

were approximately 2.5 times larger than the polyethylenes produced using parent complex **A**_{sMAO} (76 kg mol⁻¹ at 80 °C).[35] Similarly to **A**_{sMAO}, the polymers produced using **3**_{sMAO} and **5**_{sMAO} displayed low molecular weight distributions ($M_w/M_n = 3.0\text{--}4.3$ and $2.8\text{--}3.1$ respectively), indicating that the species behave largely as single-site catalysts.

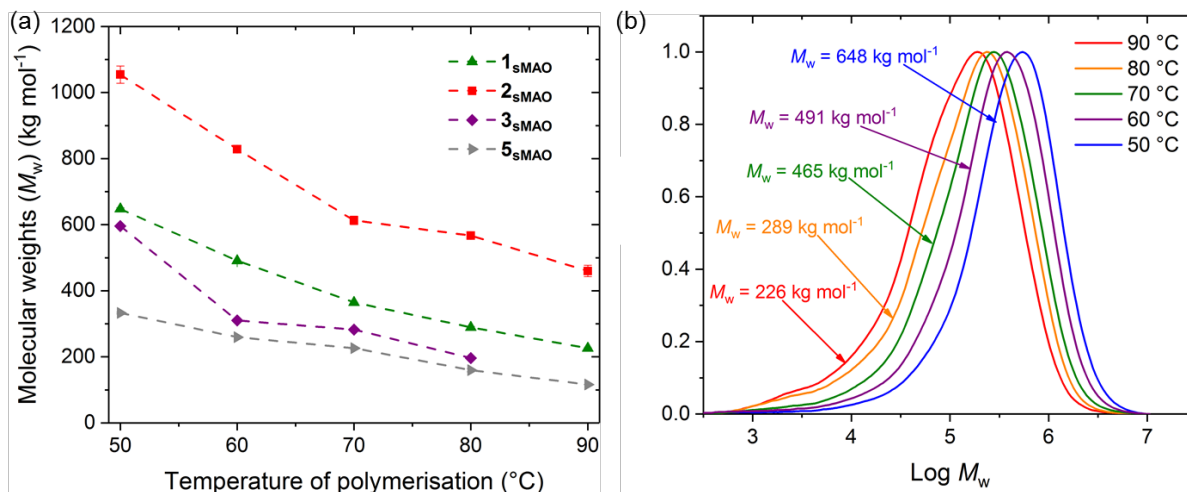


Figure 6 (a) Molecular weights (M_w) as a function of temperature of polymerisation using sMAO supported $\text{Me}_4\text{DSB}(\text{Cp}, \text{I}^*)\text{ZrCl}_2$ (**1**_{sMAO}; green triangle), $\text{Me}_4\text{DSB}(\text{tBu}_2\text{Flu}, \text{I}^*)\text{ZrCl}_2$ (**2**_{sMAO}; red square), $\text{Me}_2\text{SB}(\text{Cp}, \text{I}^*)\text{Zr}(\text{CH}_2\text{SiMe}_3)_2$ (**3**_{sMAO}; purple diamond) and $\text{Me}_2\text{SB}(\text{Cp}, \text{I}^*)\text{ZrCl}(\text{O}-2,6\text{-}i\text{Pr}-\text{C}_6\text{H}_3)$ (**5**_{sMAO}; grey right triangle); (b) Molecular weights distribution for sMAO supported $\text{Me}_4\text{DSB}(\text{Cp}, \text{I}^*)\text{ZrCl}_2$ (**1**_{sMAO}) at 50 °C (blue), 60 °C (purple), 70 °C (green), 80 °C (orange) and 90 °C (red). Normalised for clarity. Polymerisation conditions: $[\text{Al}_{\text{sMAO}}]_0/[\text{Zr}]_0 = 200$, TiBA (150 mg), ethylene (2 bar), pre-catalyst (10 mg), hexane (50 mL) and 30 minutes.

Scanning electron microscopy (SEM) analysis of the polyethylenes produced using **1**_{sMAO}, **2**_{sMAO}, **3**_{sMAO}, **4**_{sMAO} and **5**_{sMAO} showed the formation of industrially desirable, uniform ‘popcorn’ morphology with good flowability,[7] mimicking the morphology of the solid support (*via* the templating effect) (Figure 7a-e).[25] **1**_{sMAO}, **2**_{sMAO} and **5**_{sMAO} showed slightly more aggregated polymer morphology than **3**_{sMAO} and **4**_{sMAO}. The uniform morphologies of the polyethylenes produced using the supported systems are in contrast to the poor morphology produced by homogeneous polymerisation using **2**, which can lead to reactor fouling and limits the large scale industrial applications of this system (Figure 7f).

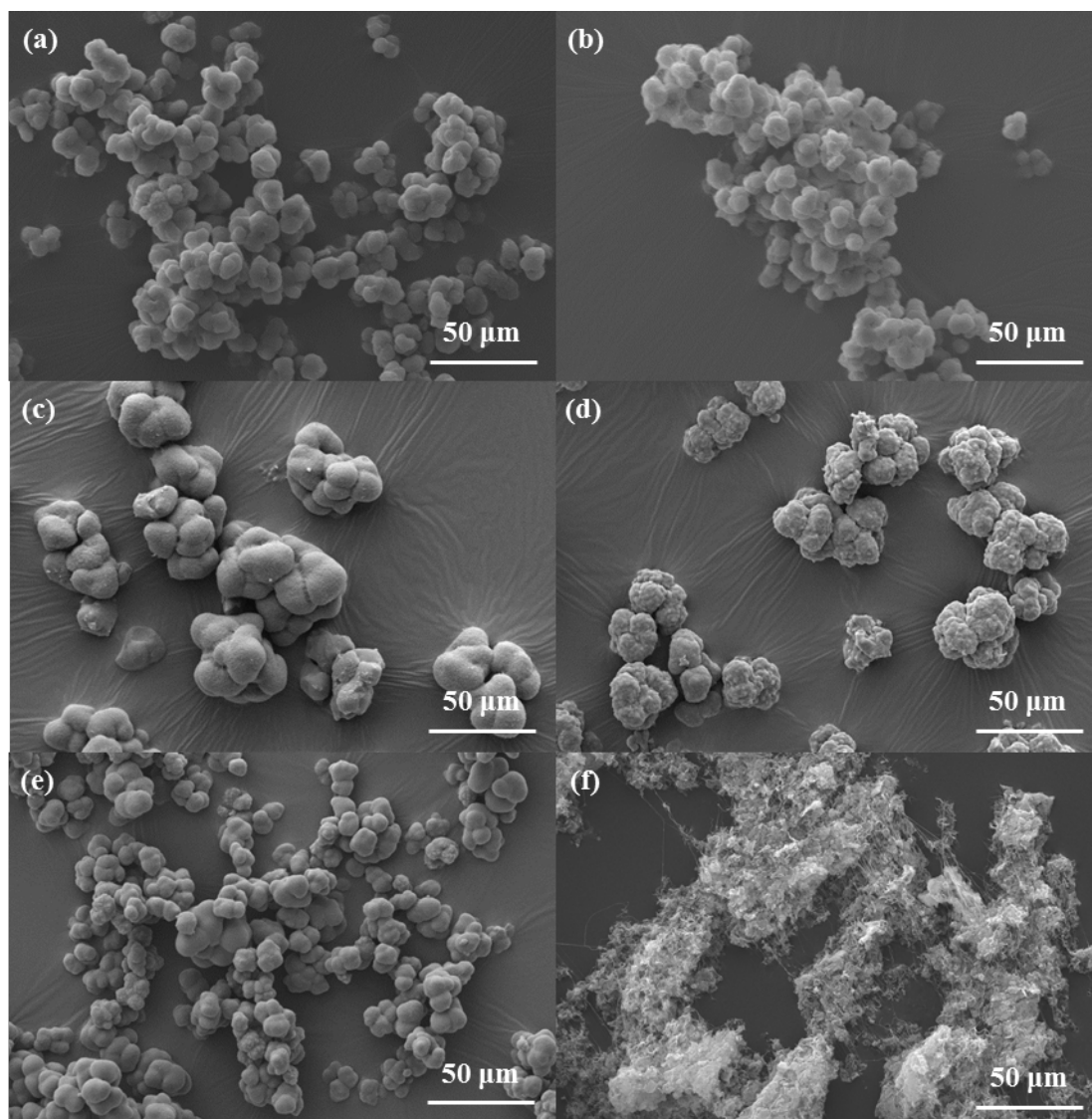


Figure 7. SEM images at $\times 500$ magnification of the polymers produced from the slurry-phase polymerisation of ethylene using (a) sMAO- $\text{Me}_4\text{DSB}(\text{Cp}, \text{I}^*)\text{ZrCl}_2$ (**1_{sMAO}**), (b) sMAO- $\text{Me}_4\text{DSB}(t\text{Bu}_2\text{Flu}, \text{I}^*)\text{ZrCl}_2$ (**2_{sMAO}**), (c) sMAO- $\text{Me}_2\text{SB}(\text{Cp}, \text{I}^*)\text{Zr}(\text{CH}_2\text{SiMe}_3)_2$ (**3_{sMAO}**), (d) sMAO- $\text{Me}_2\text{SB}(\text{Cp}^{\text{Me}}, \text{I}^*)\text{Zr}(\text{CH}_2\text{SiMe}_3)_2$ (**4_{sMAO}**), (e) sMAO- $\text{Me}_2\text{SB}(\text{Cp}, \text{I}^*)\text{ZrCl}(\text{O}-2,6\text{-}i\text{Pr}-\text{C}_6\text{H}_3)$ (**5_{sMAO}**) and (f) $\text{Me}_4\text{DSB}(t\text{Bu}_2\text{Flu}, \text{I}^*)\text{ZrCl}_2$ (**2**).

Powder X-ray diffraction (PXRD) analysis of the polymers produced using **1_{sMAO}**, **2_{sMAO}**, **3_{sMAO}** and **4_{sMAO}** in slurry-phase polymerisation showed sharp reflections at approximately 21.5° and 24.0° (corresponding to the (110) and (200) planes respectively), which is characteristic of crystalline HDPE (Figure 8).

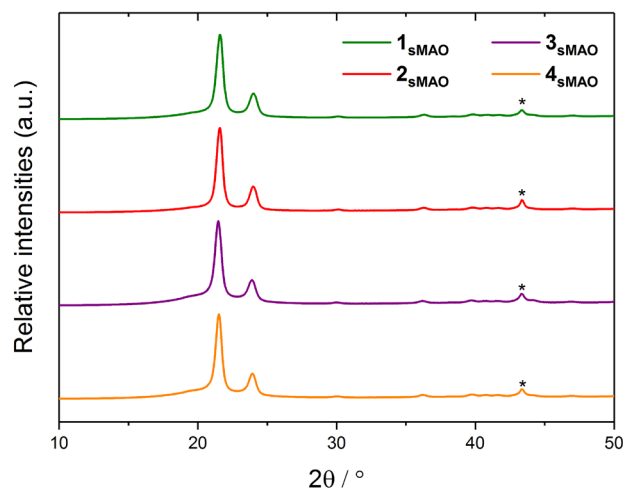


Figure 8. PXRD pattern for the polyethylenes produced using sMAO supported $\text{Me}_4\text{DSB}(\text{Cp}, \text{I}^*)\text{ZrCl}_2$ (**1_{sMAO}**) (green), $\text{Me}_4\text{DSB}(\text{tBu}_2\text{Flu}, \text{I}^*)\text{ZrCl}_2$ (**2_{sMAO}**) (red), $\text{Me}_2\text{SB}(\text{Cp}, \text{I}^*)\text{Zr}(\text{CH}_2\text{SiMe}_3)_2$ (**3_{sMAO}**) (purple) and $\text{Me}_2\text{SB}(\text{Cp}^{\text{Me}}, \text{I}^*)\text{Zr}(\text{CH}_2\text{SiMe}_3)_2$ (**4_{sMAO}**) (orange). *Denotes the reflection for the sample holder. Polymerisation conditions: $[\text{Al}_{\text{sMAO}}]_0/[\text{Zr}]_0 = 200$, TiBA (150 mg), ethylene (2 bar), pre-catalyst (10 mg), hexane (50 mL), 80 °C and 30 minutes.

DSC analysis of the polyethylenes produced by **1_{sMAO}**, **2_{sMAO}**, **3_{sMAO}**, **4_{sMAO}** and **5_{sMAO}** in slurry-phase polymerisation revealed T_m of 134–137 °C and T_c of 113–119 °C (Figure 9 and Table S11), further confirming the production of HDPE and showing the presence of minimal defects and branching.[50, 51] For the polyethylenes produced by **1_{sMAO}**, **2_{sMAO}**, **3_{sMAO}**, **4_{sMAO}** and **5_{sMAO}**, ΔH_m and ΔH_c were calculated from the DSC plots in the range 126–167 J g⁻¹ and 132–166 J g⁻¹ respectively with 45–57% polymer crystallinity (Table S10). **3_{sMAO}** and **5_{sMAO}** displayed lower T_c and higher T_m than parent complex **A_{sMAO}**; T_c of 114, 117 and 122 °C respectively and T_m of 137, 135 and 133 °C respectively.[35] A higher T_m usually indicates a higher density polymer with fewer branches.[62] The crystallinities of the polymers produced using **3_{sMAO}** and **5_{sMAO}** were significantly lower than for the polymer produced using **A_{sMAO}** (45, 57 and 75% respectively). This is expected based on the higher molecular weights of the polymers produced from **3_{sMAO}** and **5_{sMAO}** compared to **A_{sMAO}**,[35] which can lead to more chain entanglements and hinder crystal formation and growth ($M_w = 196, 160$ and 76 kg mol^{-1} respectively at 80 °C).[53, 54]

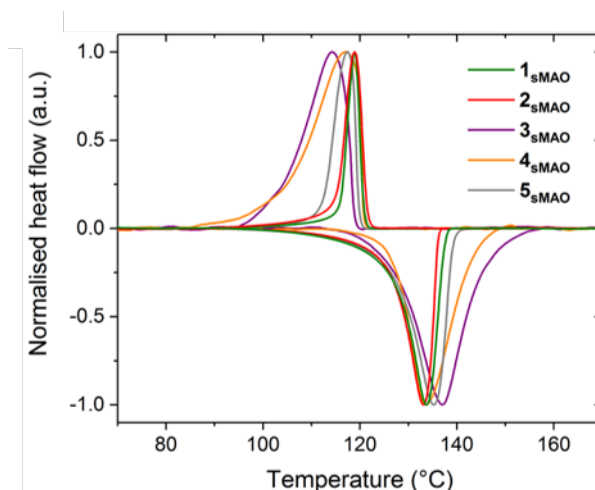


Figure 9. DSC plot showing the first cooling cycle and second heating cycle for the polyethylenes produced using sMAO supported $\text{Me}_4\text{DSB}(\text{Cp}, \text{I}^*)\text{ZrCl}_2$ (**1_{sMAO}**) (green), $\text{Me}_4\text{DSB}(\text{tBu}_2\text{Flu}, \text{I}^*)\text{ZrCl}_2$ (**2_{sMAO}**) (red), $\text{Me}_2\text{SB}(\text{Cp}, \text{I}^*)\text{Zr}(\text{CH}_2\text{SiMe}_3)_2$ (**3_{sMAO}**) (purple), $\text{Me}_2\text{SB}(\text{Cp}^{\text{Me}}, \text{I}^*)\text{Zr}(\text{CH}_2\text{SiMe}_3)_2$ (**4_{sMAO}**) (orange) and $\text{Me}_2\text{SB}(\text{Cp}, \text{I}^*)\text{ZrCl}(\text{O}-2,6\text{-}i\text{Pr}-\text{C}_6\text{H}_3)$ (**5_{sMAO}**) (grey). Normalised for clarity. Polymerisation conditions: $[\text{Al}_{\text{sMAO}}]_0/[\text{Zr}]_0 = 200$, TiBA (150 mg), ethylene (2 bar), pre-catalyst (10 mg), hexane (50 mL), 80 °C and 30 minutes.

3.3 Polymerisation studies using LDHMAO

Recently, the use of MAO-activated thermally treated aqueous miscible organic solvent treated layered double hydroxides (LDHMAO) as well-defined supports for the immobilisation of single-site α -olefin polymerisation catalysts has emerged.[35, 63, 64] Aqueous miscible organic solvent treated layered double hydroxides (AMO-LDHs) are the product of an aqueous miscible organic solvent treatment (AMOST) method, where the AMO solvent is typically acetone or ethanol. The resulting crystalline AMO-LDHs display uniform particle sizes smaller than 0.5 μm and possess surface areas and pore volumes significantly higher than conventional and commercial LDHs.[65, 66] AMO-LDH supports are industrially desirable as they are simple to synthesise on a large scale, more cost-effective than silica and show no evidence of reactor fouling or catalyst leaching.[65]

Complex **3** was immobilised onto LDHMAO ($\text{Mg}_2\text{Al-CO}_3$) (**3_{LDHMAO}**) with $[\text{Al}_{\text{sMAO}}]_0/[\text{Zr}]_0 = 200$ following an analogous procedure to sMAO. Characterisation of **3_{LDHMAO}** was achieved using SSNMR spectroscopy (Figures S26-S28). Similarly to **3_{sMAO}**, the ^{13}C CP/MAS SSNMR spectrum of **3_{LDHMAO}** shows a dominant resonance at approximately -8 ppm corresponding to the methyl groups present within MAO, weak resonances between 15 and 75 ppm corresponding to the methyl groups of the silyl bridge, indenyl rings and neosilyl

ligand, and weak resonances between 120 and 140 ppm corresponding to the carbon atoms of the arene rings. In addition, the spectrum also shows a dominant resonance at 167 ppm corresponding to the carbonate within LDHMAO support (Figure S26). The ^{29}Si CP/MAS SSNMR spectrum shows two resonances at -13.6 and 0.8 ppm corresponding to the silicon atoms of the neosilyl ligand and bridge respectively (Figure S27), while the ^{27}Al DP/MAS SSNMR spectrum shows a series of broad resonances between -245 and 450 ppm (Figure S28).

3_{LDHMAO} displayed a peak polymerisation activity of $4747 \text{ kg}_{\text{PE}} \text{ mol}_{\text{Zr}}^{-1} \text{ h}^{-1} \text{ bar}^{-1}$ respectively at 70°C ; similar to that of **3**_{sMAO} ($4191 \text{ kg}_{\text{PE}} \text{ mol}_{\text{Zr}}^{-1} \text{ h}^{-1} \text{ bar}^{-1}$) (Figure 10 and Table S9). **3**_{LDHMAO} displayed much higher slurry-phase ethylene polymerisation activities than **1**_{LDHMAO} and LDHMAO supported ($^{2-\text{Me},4-\text{Ph}}\text{SBI}$)ZrCl₂ (4253 , 68 and $3226 \text{ kg}_{\text{PE}} \text{ mol}_{\text{Zr}}^{-1} \text{ h}^{-1} \text{ bar}^{-1}$ respectively at 60°C).^[35, 64] **3**_{LDHMAO} also displayed slurry-phase ethylene polymerisation activities approximately double that of industrial standard ($\text{Cp}^{n\text{Bu}}\text{)}_2\text{ZrCl}_2$ supported on LDHMAO (4253 and $2141 \text{ kg}_{\text{PE}} \text{ mol}_{\text{Zr}}^{-1} \text{ h}^{-1} \text{ bar}^{-1}$ at 60°C).^[64]

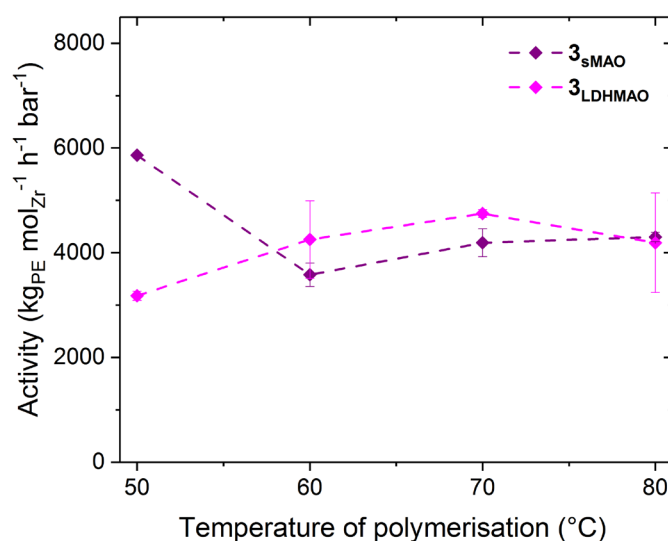


Figure 10. Slurry-phase ethylene polymerisation activity as a function of temperature of polymerisation using sMAO-^{Me}₂SB(Cp,I*)Zr(CH₂SiMe₃)₂ (**3**_{sMAO}) (purple) and LDHMAO-^{Me}₂SB(Cp,I*)Zr(CH₂SiMe₃)₂ (**3**_{LDHMAO}) (pink). Polymerisation conditions: $[\text{Al}_{\text{support}}]_0/[\text{Zr}]_0 = 200$, TiBA (150 mg), ethylene (2 bar), pre-catalyst (10 mg), hexane (50 mL) and 30 minutes.

SEM analysis of the polyethylenes produced using **3**_{LDHMAO} showed the formation of aggregated, non-uniform polymer particles, mimicking the morphology of the solid support

(Figure 11). The same effect was also observed for $\text{Me}_2\text{SB}(\text{Cp}^{\text{R}}, \text{I}^*)\text{ZrCl}_2$ ($\text{R} = \text{H}$ and Me) and $\text{Me}_2\text{SB}(\text{}^i\text{BuFlu}, \text{I}^*)\text{ZrCl}_2$ supported on sMAO and LDHMAO.[7, 35] The flowability of the polymer produced using $\mathbf{3}_{\text{LDHMAO}}$ was reduced when compared to $\mathbf{3}_{\text{sMAO}}$, likely due to the more aggregated morphology of the LDHMAO support leading to a poorer templating effect.[35]

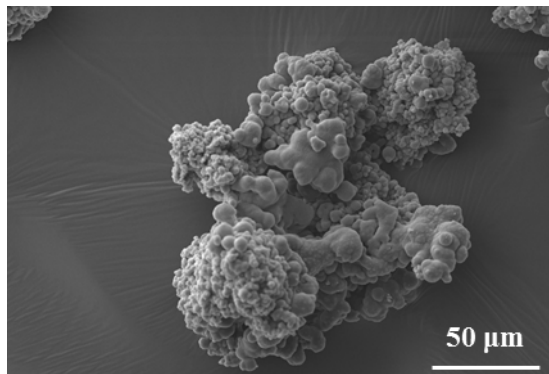


Figure 11. SEM image at $\times 500$ magnification of the polymers produced from the slurry-phase polymerisation of ethylene using LDHMAO- $\text{Me}_2\text{SB}(\text{Cp}, \text{I}^*)\text{Zr}(\text{CH}_2\text{SiMe}_3)_2$ ($\mathbf{3}_{\text{LDHMAO}}$).

DSC analysis of the polyethylenes produced by $\mathbf{3}_{\text{LDHMAO}}$ revealed T_{m} and T_{c} identical to the polyethylenes produced using $\mathbf{3}_{\text{sMAO}}$ (137 and 114 °C respectively) (Figure 12); confirming the production of HDPE with minimal defects and branching.[50, 51] The enthalpy of melting (ΔH_{m}) and cooling (ΔH_{c}) were calculated as 105 J g $^{-1}$ and 128 J g $^{-1}$ respectively with polymer crystallinity similar to the polyethylenes produced using $\mathbf{3}_{\text{sMAO}}$ (44 and 45%) respectively.

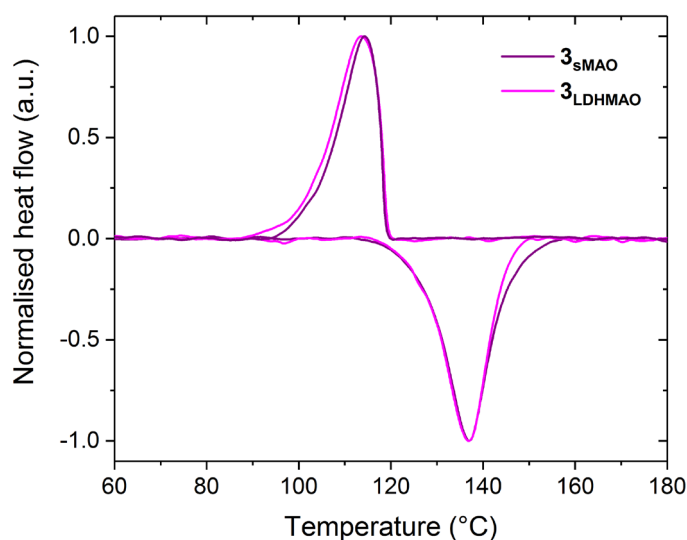


Figure 12. DSC plot showing the first cooling cycle and second heating cycle for the polyethylenes produced using sMAO-^{Me}₂SB(Cp,I*)Zr(CH₂SiMe₃)₂ (**3**_{sMAO}) (purple) and LDHMAO-^{Me}₂SB(Cp,I*)Zr(CH₂SiMe₃)₂ (**3**_{LDHMAO}) (pink). Normalised for clarity. Polymerisation conditions: [Al_{support}]₀/[Zr]₀ = 200, TiBA (150 mg), ethylene (2 bar), pre-catalyst (10 mg), hexane (50 mL), 80 °C, 30 minutes.

4. Conclusions

Five new permethylindenyl zirconocene complexes have been synthesised and fully characterised: ^{Me}₄DSB(Cp,I*)ZrCl₂ (**1**), ^{Me}₄DSB(^tBu₂Flu,I*)ZrCl₂ (**2**), ^{Me}₂SB(Cp,I*)Zr(SiMe₃)₂ (**3**), ^{Me}₂SB(Cp^{Me},I*)Zr(SiMe₃)₂ (**4**) and ^{Me}₂SB(Cp,I*)ZrCl(O-2,6-ⁱPr-C₆H₃) (**5**). The complexes were immobilised on solid polymethylaluminumoxane (sMAO) and the slurry-phase ethylene polymerisation activity studied at various temperatures.

4_{sMAO} displayed the highest ethylene polymerisation activity (8042 kg_{PE} mol_{Zr}⁻¹ h⁻¹ bar⁻¹ at 60 °C); 73% more active than an industrial standard, sMAO-(CpⁿBu)₂ZrCl₂, under the same conditions. The polyethylenes produced using **1**_{sMAO}, **2**_{sMAO}, **3**_{sMAO} and **5**_{sMAO} showed relatively low molecular weights $M_w < 650$ kg mol⁻¹ at 80 °C. **1**_{sMAO} and **2**_{sMAO} produced polymers with wide molecular weight distributions ($M_w/M_n = 6.7\text{--}8.1$ and $8.4\text{--}17.9$ respectively) implying that a variety of surface sites may exist, while **3**_{sMAO} and **5**_{sMAO} produced polymers low molecular weight distributions ($M_w/M_n = 3.0\text{--}4.3$ and $2.8\text{--}3.1$ respectively) indicating that the species behave largely as single-site catalysts. SEM analysis of the polyethylenes showed the formation of industrially desirable, uniform, ‘popcorn’ morphology in all cases.

^{Me}₂SB(Cp,I*)Zr(SiMe₃)₂ (**3**) was also immobilised on MAO modified layered double hydroxide (LDHMAO). Polymerisation activity was similar to the same complex immobilised on sMAO, however polymer morphology was much more aggregated and less uniform.

5. Experimental

5.1 Synthesis of Ind*(SiMe₂)₂Cl

1.0 equivalent Ind[#]H (10.0 g, 50.0 mmol) was dissolved in pentane (100 mL). The solution was cooled to 0 °C and 1.1 equivalents ⁿBuLi (22.0 mL, 2.5 M in hexanes, 55.0 mmol) added dropwise. The reaction was allowed to warm to room temperature, stirred for 18 h and the solvent removed *in vacuo*. The resulting lithium salt was dissolved in THF (100 mL) and added dropwise to a solution of 3.0 equivalents (Me₂SiCl)₂ (27.9 mL, 150.3 mmol). The reaction was stirred for 2 h, the solvent removed and the product extracted with pentane (2 × 30 mL).

Storage at $-34\text{ }^{\circ}\text{C}$ yielded $\text{Ind}^*(\text{SiMe}_2)_2\text{Cl}$ as a pale yellow solid in 70% yield (12.3 g, 35.0 mmol). ^1H NMR ($\text{C}_4\text{D}_8\text{O}$, 400 MHz, 298 K) δ (ppm): 3.56 (SiCH, 1H, s), 2.49 (C=CMe, 3H, s), 2.24 (ArMe, 3H, s), 2.22 (ArMe, 3H, s), 2.21 (ArMe, 3H, s), 2.20 (ArMe, 3H, s), 2.10 (C=CMe, 3H, s), 0.36 (SiMe, 3H, s), 0.24 (SiMe, 3H, s), 0.20 (SiMe, 3H, s) and -0.21 (SiMe, 3H, s). $^{13}\text{C}\{^1\text{H}\}$ NMR ($\text{C}_4\text{D}_8\text{O}$, 125 MHz, 298 K) δ (ppm): 143.1 (Ar), 141.7 (Ar), 141.0 (Ar), 133.2 (Ar), 133.0 (Ar), 130.9 (Ar), 127.7 (Ar), 127.2 (Ar), 47.9 (ArSi), 19.3 (ArMe), 16.5 (ArMe), 16.4 (ArMe), 15.8 (ArMe), 15.7 (ArMe), 3.2 (SiMe), 2.4 (SiMe), -1.2 (SiMe) and -1.6 (SiMe).

5.2 Synthesis of $^{\text{Me}_4}\text{DSB}(\text{Cp}, \text{I}^*)\text{Li}_2$

1.0 equivalent LiCp (0.205 g, 2.85 mmol) and 1.0 equivalent $\text{Ind}^*(\text{SiMe}_2)_2\text{Cl}$ (1.00 g, 2.85 mmol) were dissolved in THF (20 mL) and stirred for 2 h at room temperature. 2.2 equivalents $n\text{BuLi}$ (3.9 mL, 1.6 M in hexane, 6.27 mmol) were added drop-wise at $0\text{ }^{\circ}\text{C}$, after which the reaction mixture was allowed to warm to room temperature and stirred for 1 hour. The solvent was removed *in vacuo* and the residue washed with pentane ($3 \times 20\text{ mL}$) and diethyl ether ($3 \times 30\text{ mL}$). The resulting solid was dried to afford $^{\text{Me}_4}\text{DSB}(\text{Cp}, \text{I}^*)\text{Li}_2$ as a brown powder in 78% yield (0.880 g, 2.24 mmol). ^1H NMR ($\text{C}_5\text{D}_5\text{N}$, 400 MHz, 298 K) δ (ppm): 6.56 (CpH, 2H, m), 6.27 (CpH, 2H, m), 3.06 (ArMe, 3H, s), 2.84 (ArMe, 3H, s), 2.75 (ArMe, 3H, s), 2.73 (ArMe, 3H, s), 2.43 (ArMe, 3H, s), 2.39 (ArMe, 3H, s), 0.92 (SiMe, 6H, s) and 0.83 (SiMe, 6H, s). $^{13}\text{C}\{^1\text{H}\}$ NMR ($\text{C}_5\text{D}_5\text{N}$, 125 MHz, 298 K) δ (ppm): 136.0 (Ar), 135.0 (Ar), 134.2 (Ar), 131.0 (Ar), 122.3 (Ar), 120.3 (Ar), 120.8 (Ar), 112.7 (Ar), 111.6 (Cp), 107.7 (Cp), 105.7 (CpSi), 89.6 (ArSi), 24.0 (ArMe), 18.5 (ArMe), 17.9 (ArMe), 17.8 (ArMe), 17.2 (ArMe), 16.1 (ArMe), 6.4 (SiMe) and 0.7 (SiMe).

5.3 Synthesis of $^{\text{Me}_4}\text{DSB}(^t\text{Bu}_2\text{Flu}, \text{I}^*)\text{Li}_2 \cdot (\text{Et}_2\text{O})_{1.5}$

1.0 equivalent $^t\text{Bu}_2\text{FluLi}$ (1.13 g, 2.85 mmol) and 1.0 equivalent $\text{Ind}^*(\text{SiMe}_2)_2\text{Cl}$ (1.00 g, 2.85 mmol) were dissolved in THF (30 mL) and stirred for 2 h at room temperature. 2.2 equivalents $n\text{BuLi}$ (3.9 mL, 1.6 M in hexane, 6.27 mmol) were added drop-wise at $0\text{ }^{\circ}\text{C}$, after which the reaction mixture was allowed to warm to room temperature and stirred for 1 hour. The solvent was removed *in vacuo* and the residue washed with pentane ($3 \times 50\text{ mL}$) and diethyl ether ($2 \times 50\text{ mL}$). The solid was dried to afford $^{\text{Me}_4}\text{DSB}(^t\text{Bu}_2\text{Flu}, \text{I}^*)\text{Li}_2 \cdot (\text{Et}_2\text{O})_{1.5}$ as a yellow solid in 19% yield (0.381 g, 0.532 mmol). ^1H NMR ($\text{C}_5\text{D}_5\text{N}$, 400 MHz, 298 K) δ (ppm): 8.50 (FluH, 2H, d, $^3J_{\text{H-H}} = 4\text{ Hz}$), 8.47 (FluH, 2H, s), 7.12 (FluH, 2H, dd, $^3J_{\text{H-H}} = 8.0\text{ Hz}$), 3.36 (OCH_2CH_3 , 4H, q, $^3J_{\text{H-H}} = 8\text{ Hz}$), 3.02 (ArMe, 3H, s), 2.88 (ArMe, 3H, s),

2.76 (ArMe, 3H, s), 2.75 (ArMe, 3H, s), 2.35 (ArMe, 3H, s), 2.23 (ArMe, 3H, s), 1.64 (Flu'Bu, 18H, s), 1.28 (SiMe, 6H, s), 1.14 (OCH₂CH₃, 6H, t, ³J_{H-H} = 8 Hz) and 1.07 (SiMe, 6H, s). ¹³C{¹H} NMR (C₅D₅N, 125 MHz, 298 K) δ (ppm): 149.8 (Ar), 146.2 (Ar), 141.4 (Ar), 136.5 (Ar), 135.1 (Ar), 126.0 (Ar), 124.5 (Ar), 124.4 (Ar), 124.1 (Ar), 123.9 (Ar), 123.4 (Ar), 119.1 (FluH), 116.1 (FluH), 108.7 (FluH), 105.2 (ArSi), 66.3 (OCH₂CH₃), 35.7 (FluSi), 33.4 (Flu'Bu), 26.3 (ArMe), 23.6 (ArMe), 18.3 (ArMe), 17.5 (ArMe), 17.0 (ArMe), 16.2 (ArMe), 16.0 (OCH₂CH₃), 7.0 (SiMe) and 3.4 (SiMe).

5.4 Synthesis of ^{Me}₄DSB(Cp,I*)ZrCl₂ (**1**)

1.0 equivalent ^{Me}₄DSB(Cp,I*)Li₂ (0.880 g, 2.24 mmol) and 1.0 equivalent ZrCl₄ (0.520 g, 2.24 mmol) were dissolved in benzene (30 mL) and stirred at room temperature for 18 h. The resulting orange solution was filtered, the solvent removed and the product extracted with pentane (3 × 20 mL). The insoluble orange solid was shown by ¹H NMR spectroscopy to be the desired product in 7% yield (0.086 g, 0.159 mmol). Storage of the pentane solution at −34 °C yielded another crop of ^{Me}₄DSB(Cp,I*)ZrCl₂ (**1**) as an orange solid in 13% yield (0.122 g, 226 mmol). ¹H NMR (C₆D₆, 400 MHz, 298 K) δ (ppm): 6.84 (CpH, 1H, m), 6.41 (CpH, 1H, m), 5.74 (CpH, 1H, m), 5.67 (CpH, 1H, m), 2.63 (ArMe, 3H, s), 2.62 (ArMe, 3H, s), 2.60 (ArMe, 3H, s), 2.30 (ArMe, 3H, s), 2.01 (ArMe, 3H, s), 1.98 (ArMe, 3H, s), 0.60 (SiMe, 3H, s), 0.46 (SiMe, 3H, s), 0.37 (SiMe, 3H, s) and 0.35 (SiMe, 3H, s). ¹³C{¹H} NMR (C₆D₆, 125 MHz, 298 K) δ (ppm): 147.7 (Ar), 133.4 (Ar), 132.5 (Ar), 132.3 (Ar), 131.9 (Ar), 131.0 (Ar), 130.9 (Ar), 129.9 (Ar), 123.0 (Cp), 120.4 (Cp), 119.8 (Cp), 119.4 (Cp), 115.9 (CpSi), 102.6 (ArSi), 23.6 (ArMe), 18.0 (ArMe), 17.3 (ArMe), 17.0 (ArMe), 16.7 (ArMe), 15.0 (ArMe), 5.0 (SiMe), 3.6 (SiMe), −1.0 (SiMe) and −2.3 (SiMe). ²⁹Si NMR (C₆D₆, 100 MHz, 298 K) δ (ppm): −17.0 (SiMe) and −21.7 (SiMe). CHN Analysis (%): expected C 53.41, H 6.46, observed C 53.47, H 6.50. CCDC number: 1958152.

5.5 Synthesis of ^{Me}₄DSB(^tBu₂Flu,I*)ZrCl₂ (**2**)

1.0 equivalent ^{Me}₄DSB(^tBu₂Flu,I*)Li₂·(Et₂O)_{1.5} (0.380 g, 0.530 mmol) and 1.0 equivalent ZrCl₄ (0.120 g, 0.530 mmol) were dissolved in benzene (30 mL) and stirred for 18 h at room temperature. The resulting orange solution was filtered, the solvent removed and the product extracted with pentane (3 × 20 mL). The insoluble orange powder was shown by ¹H NMR spectroscopy to be the desired product in 22% yield (0.086 g, 0.114 mmol). Storage of the filtrate at −80 °C yielded another crop of ^{Me}₄DSB(^tBu₂Flu,I*)ZrCl₂ (**2**) as orange crystals suitable for a single crystal X-ray diffraction study in 52% yield (0.122 g, 0.162 mmol). ¹H NMR (C₆D₆,

400 MHz, 298 K) δ (ppm): 7.86 (FluH, 1H, d, $^3J_{\text{H-H}} = 8$ Hz), 7.70 (FluH, 1H, d, $^3J_{\text{H-H}} = 8$ Hz), 7.69 (FluH, 1H, s), 7.62 (FluH, 1H, s), 7.59 (FluH, 1H, dd, $^3J_{\text{H-H}} = 8$ Hz), 7.40 (FluH, 1H, dd, $^3J_{\text{H-H}} = 8$ Hz), 2.84 (ArMe, 3H, s), 2.35 (ArMe, 3H, s), 2.32 (ArMe, 3H, s), 2.06 (ArMe, 3H, s), 2.03 (ArMe, 3H, s), 2.02 (ArMe, 3H, s), 1.40 (Flu'Bu, 9H, s), 1.32 (Flu'Bu, 9H, s), 0.86 (SiMe, 3H, s), 0.86 (SiMe, 3H, s), 0.71 (SiMe, 3H, s) and 0.67 (SiMe, 3H, s). $^{13}\text{C}\{^1\text{H}\}$ NMR (C_6D_6 , 125 MHz, 298 K) δ (ppm): 150.5 (Flu'Bu), 149.3 (Flu'Bu), 135.2 (Ar), 134.0 (Ar), 133.5 (Ar), 133.3 (Ar), 132.4 (Ar), 131.1 (Ar), 130.5 (Flu), 129.8 (Flu), 129.7 (Flu), 127.4 (Ar), 127.0 (Ar), 126.0 (FluH), 125.8 (FluH), 125.3 (FluH), 124.5 (FluH), 121.3 (FluH), 120.4 (FluH), 105.6 (ArSi), 89.2 (FluSi), 35.4 (Flu'Bu), 35.4 (Flu'Bu), 31.4 (Flu'Bu), 31.3 (Flu'Bu), 24.3 (ArMe), 17.8 (ArMe), 17.5 (ArMe), 17.2 (ArMe), 16.5 (ArMe), 16.2 (ArMe), 4.9 (SiMe), 4.6 (SiMe), 1.4 (SiMe) and 1.0 (SiMe). CHN Analysis (%): expected C 63.72, H 7.27, observed C 63.72, H 7.34.

5.6 Synthesis of $^{\text{Me}_2}\text{SB}(\text{Cp}, \text{I}^*)\text{Zr}(\text{CH}_2\text{SiMe}_3)_2$ (**3**)

1.0 equivalent $^{\text{Me}_2}\text{SB}(\text{Cp}, \text{I}^*)\text{ZrCl}_2$ (0.200 g, 0.400 mmol) and 2.5 equivalents $\text{LiCH}_2\text{SiMe}_3$ (0.096 g, 1.00 mmol) were dissolved in benzene (40 mL) and stirred for four days at room temperature. The solution was filtered, the solvent removed *in vacuo* and the resultant dark orange solid extracted with pentane (2×15 mL). Storage of the yellow filtrate at -34 °C yielded $^{\text{Me}_2}\text{SB}(\text{Cp}, \text{I}^*)\text{Zr}(\text{CH}_2\text{SiMe}_3)_2$ (**3**) as a yellow solid in 12% yield (0.030 g, 0.050 mmol). ^1H NMR (C_6D_6 , 500 MHz, 298 K) δ (ppm): 6.90 (CpH, 1H, m), 6.72 (CpH, 1H, m), 5.82 (CpH, 1H, m), 5.20 (CpH, 1H, m), 2.50 (ArMe, 3H, s), 2.40 (ArMe, 3H, s), 2.17 (ArMe, 3H, s), 2.11 (ArMe, 3H, s), 2.07 (ArMe, 3H, s), 1.90 (ArMe, 3H, s), 0.63 (SiMe, 3H, s), 0.62 (SiMe, 3H, s), 0.21 (CH_2SiMe , 9H, s), 0.08 (CHSiMe , 1H, d, $^2J_{\text{H-H}} = 10$ Hz), -0.02 (CH_2SiMe , 9H, s), -0.52 (CHSiMe , 1H, d, $^2J_{\text{H-H}} = 10$ Hz), -1.11 (CHSiMe , 1H, d, $^2J_{\text{H-H}} = 10$ Hz) and -2.49 (CHSiMe , 1H, d, $^2J_{\text{H-H}} = 10$ Hz). $^{13}\text{C}\{^1\text{H}\}$ NMR (C_6D_6 , 125 MHz, 298 K) δ (ppm): 133.5 (Ar), 132.9 (Ar), 132.1 (Ar), 130.3 (Ar), 129.7 (Ar), 129.4 (Ar), 126.6 (Ar), 121.8 (Ar), 118.7 (Cp), 115.8 (Cp), 113.9 (Cp), 111.1 (Cp), 103.1 (CpSi), 79.1 (ArSi), 46.3 (CH_2SiMe), 46.2 (CH_2SiMe), 21.4 (ArMe), 17.4 (ArMe), 17.3 (ArMe), 16.8 (ArMe), 16.5 (ArMe), 15.7 (ArMe), 4.7 (SiMe), 4.1 (CH_2SiMe), 3.6 (SiMe) and 3.1 (CH_2SiMe).

5.7 Synthesis of $^{\text{Me}_2}\text{SB}(\text{Cp}^{\text{Me}}, \text{I}^*)\text{Zr}(\text{CH}_2\text{SiMe}_3)_2$ (**4**)

1.0 equivalent $^{\text{Me}_2}\text{SB}(\text{Cp}^{\text{Me}}, \text{I}^*)\text{ZrCl}_2$ (0.204 g, 0.400 mmol) and 2.5 equivalents $\text{LiCH}_2\text{SiMe}_3$ (0.0960 mg, 1.00 mmol) were dissolved in benzene (40 mL) and stirred for four days at room temperature. The solution was filtered, the solvent removed *in vacuo* and the resultant dark

orange solid extracted with pentane (2×15 mL). Storage of the yellow filtrate at -34 °C yielded $\text{Me}_2\text{SB}(\text{Cp}^{\text{Me}}, \text{I}^*)\text{Zr}(\text{CH}_2\text{SiMe}_3)_2$ (**4**) as a yellow solid in 53% yield (0.132 g, 0.220 mmol). *Isomer A*: ^1H NMR (C_6D_6 , 500 MHz, 298 K) δ (ppm): 6.46 (CpH, 1H, m), 5.92 (CpH, 1H, m), 4.94 (CpH, 1H, m), 2.55 (ArMe, 3H, s), 2.21 (ArMe, 6H, s), 2.38 (ArMe, 3H, s), 2.20 (ArMe, 3H, s), 2.17 (ArMe, 3H, s), 1.83 (ArMe, 3H, s), 0.64 (SiMe, 3H, s), 0.63 (SiMe, 3H, s), 0.24 (CHSiMe, 1H, d, $^2J_{\text{H-H}} = 10$ Hz), 0.21 (CH₂SiMe, 9H, s), 0.03 (CH₂SiMe, 9H, s), -0.90 (CHSiMe, 1H, d, $^2J_{\text{H-H}} = 10$ Hz), -0.99 (CHSiMe, 1H, d, $^2J_{\text{H-H}} = 10$ Hz) and -2.60 (CHSiMe, 1H, d, $^2J_{\text{H-H}} = 10$ Hz). $^{13}\text{C}\{^1\text{H}\}$ NMR (C_6D_6 , 125 MHz, 298 K) δ (ppm): 122.5 (CpMe), 114.7 (Cp), 113.5 (Cp), 112.7 (Cp), 101.5 (CpSi), 78.6 (ArSi), 54.1 (CH₂SiMe), 40.2 (CH₂SiMe), 21.2 (CpMe), 17.7 (ArMe), 16.8 (ArMe), 16.8 (ArMe), 16.3 (ArMe), 15.8 (ArMe), 15.5 (ArMe), 5.0 (SiMe), 3.9 (CH₂SiMe), 3.7 (SiMe) and 3.1 (CH₂SiMe). Ar resonances cannot be further assigned to the separate isomers (133.3, 133.3, 132.9, 132.4, 132.4, 132.2, 131.9, 130.8, 129.8, 129.8, 129.6, 129.5, 129.2, 127.4, 127.0, 126.9). *Isomer B*: ^1H NMR (C_6D_6 , 500 MHz, 298 K) δ (ppm): 6.70 (CpH, 1H, m), 5.51 (CpH, 1H, m), 5.22 (CpH, 1H, m), 2.60 (ArMe, 3H, s), 2.48 (ArMe, 3H, s), 2.14 (ArMe, 3H, s), 2.13 (ArMe, 3H, s), 2.09 (ArMe, 6H, s), 1.98 (ArMe, 3H, s), 0.69 (CHSiMe, 1H, d, $^2J_{\text{H-H}} = 10$ Hz), 0.69 (SiMe, 3H, s), 0.68 (SiMe, 3H, s), 0.24 (CH₂SiMe, 9H, s), 0.00 (CH₂SiMe, 9H, s), -0.65 (CHSiMe, 1H, d, $^2J_{\text{H-H}} = 10$ Hz), -0.79 (CHSiMe, 1H, d, $^2J_{\text{H-H}} = 10$ Hz) and -2.49 (CHSiMe, 1H, d, $^2J_{\text{H-H}} = 10$ Hz). $^{13}\text{C}\{^1\text{H}\}$ NMR (C_6D_6 , 125 MHz, 298 K) δ (ppm): 121.4 (CpMe), 118.7 (Cp), 117.0 (Cp), 110.5 (Cp), 102.8 (CpSi), 79.7 (ArSi), 52.7 (CH₂SiMe), 40.0 (CH₂SiMe), 21.7 (ArMe), 18.2 (ArMe), 17.5 (ArMe), 17.3 (ArMe), 17.1 (ArMe), 16.1 (CpMe), 15.9 (ArMe), 4.4 (SiMe), 4.4 (CH₂SiMe) and 3.9 (SiMe), 3.5 (CH₂SiMe). Ar resonances cannot be further assigned to the separate isomers (133.3, 133.3, 132.9, 132.4, 132.4, 132.2, 131.9, 130.8, 129.8, 129.8, 129.6, 129.5, 129.2, 127.4, 127.0, 126.9). *Isomeric Mixture*: CHN Analysis (%): expected C 48.30, H 7.37; observed C 48.37, H 7.46.

5.8 Synthesis of $\text{Me}_2\text{SB}(\text{Cp}, \text{I}^*)\text{ZrCl}(\text{O}-2,6\text{-}^i\text{Pr}-\text{C}_6\text{H}_3)$ (**5**)

$\text{Me}_2\text{SB}(\text{Cp}, \text{I}^*)\text{ZrCl}_2$ (0.300 g, 0.620 mmol) and 2.2 equivalents $\text{K}(\text{O}-2,6\text{-}^i\text{Pr}-\text{C}_6\text{H}_3)$ (0.296 g, 1.37 mmol) were dissolved in benzene (20 mL) and stirred at room temperature for 16 h. Filtration and removal of solvent *in vacuo* yielded an orange oil and the crude ^1H NMR spectra showed resonances corresponding to a mixture of two isomers. Extraction in pentane (2×20 mL) and storage at -34 °C overnight yielded a single isomer of $\text{Me}_2\text{SB}(\text{Cp}, \text{I}^*)\text{ZrCl}(\text{O}-2,6\text{-}^i\text{Pr}-\text{C}_6\text{H}_3)$ (**5**) with the aryloxide ligand positioned away from the I^* ligand (*E*-isomer) as yellow crystals suitable for a single crystal X-ray diffraction study in 14%

yield (0.056 g, 0.090 mmol). *E*-Isomer: ^1H NMR (C_6D_6 , 400 MHz, 298 K) δ (ppm): 7.14 (OArH, 2H, d, $^3J_{\text{H-H}} = 8$ Hz), 7.12 (OArH, 2H, d, $^3J_{\text{H-H}} = 8$ Hz), 6.99 (OArH, 1H, t, $^3J_{\text{H-H}} = 8$ Hz), 6.40 (CpH, 1H, m), 6.26 (CpH, 1H, m), 5.89 (CpH, 1H, m), 5.71 (CpH, 1H, m), 3.61 (OArCHMe₂, 1H, sept, $^3J_{\text{H-H}} = 8$ Hz), 3.07 (OArCHMe₂, 1H, sept, $^3J_{\text{H-H}} = 8$ Hz), 2.46 (ArMe, 3H, s), 2.31 (ArMe, 3H, s), 2.25 (ArMe, 3H, s), 2.21 (ArMe, 3H, s), 2.18 (ArMe, 3H, s), 2.15 (ArMe, 3H, s), 1.30 (OArCHMe, 12H, m), 0.77 (SiMe, 3H, s) and 0.66 (SiMe, 3H, s). $^{13}\text{C}\{^1\text{H}\}$ NMR (C_6D_6 , 125 MHz, 298 K) δ (ppm): 158.9 (OAr), 138.5 (OAr^{*i*}Pr), 136.9 (Ar), 135.5 (Ar), 134.8 (OAr^{*i*}Pr), 133.9 (Ar), 133.9 (Ar), 129.7 (Ar), 129.5 (Ar), 128.2 (Ar), 126.9 (Ar), 125.1 (Cp), 123.9 (OArH), 123.8 (OArH), 120.6 (OArH), 120.1 (Cp), 120.0 (Cp), 113.1 (CpSi), 109.1 (Cp), 85.8 (ArSi), 27.4 (OArCHMe), 25.7 (OArCH), 25.3 (OArCHMe), 25.0 (OArCH), 23.7 (OArCHMe), 23.0 (OArCHMe), 21.2 (ArMe), 17.5 (ArMe), 17.4 (ArMe), 16.7 (ArMe), 16.6 (ArMe), 15.1 (ArMe), 4.4 (SiMe) and 3.2 (SiMe). *Z*-Isomer: ^1H NMR (benzene-*d*₆, 400 MHz, 298 K) δ (ppm): 7.05 (OArH, 2H, m), 6.83 (OArH, 1H, t, $^3J_{\text{H-H}} = 8$ Hz), 6.79 (CpH, 1H, m), 6.19 (CpH, 1H, m), 6.12 (CpH, 1H, m), 5.61 (CpH, 1H, m), 3.56 (OArCHMe₂, 1H, sept, $^3J_{\text{H-H}} = 10$ Hz), 2.93 (OArCHMe₂, 1H, sept, $^3J_{\text{H-H}} = 10$ Hz), 2.57 (ArMe, 3H, s), 2.42 (ArMe, 3H, s), 2.35 (ArMe, 3H, s), 1.99 (ArMe, 3H, s), 1.88 (ArMe, 3H, s), 1.66 (ArMe, 3H, s), 1.15 (OArCHMe, 12H, m), 0.85 (SiMe, 3H, s) and 0.69 (SiMe, 3H, s). CCDC number: 1958153.

5.9 Synthesis of LDHMAO

Toluene (40 mL) was added to 1.0 equivalent thermally treated (150 °C for 6 hours) LDH ($\text{Mg}_3\text{Al-CO}_3$) and 0.5 equivalents MAO and the mixture heated at 80 °C for 2 h with swirling. The colourless solid was allowed to settle, the solution decanted and the product dried under vacuum to give the activated support in quantitative yield.

5.10 Synthesis of solid pre-catalysts

Dried solid polymethylaluminumoxane or LDHMAO and complex ($[\text{Al}_{\text{support}}]_0/[\text{Zr}]_0 = 200$) were slurried in toluene (40 mL) and heated at 60 °C for 1 h with swirling. The coloured solid was allowed to settle and the clear, colourless supernatant decanted. The solid was dried *in vacuo* to give the product as a faintly coloured powder in quantitative yield.

sMAO-Me^{*i*}DSB(Cp,I*)ZrCl₂ (1_{sMAO}): ^{13}C CP/MAS NMR (10 kHz, 298 K) δ (ppm): 137.1, 135.8, 135.3, 131.8, 128.3, 17.1, 16.0 and -7.7. ^{29}Si CP/MAS NMR (10 kHz, 298 K) δ (ppm): -12.7. ^{27}Al DP/MAS NMR (15 kHz, 298 K) δ (ppm): 345.8, 206.1, 71.6, -82.0 and -239.1.

sMAO-Me⁴DSB(^{*t*}Bu₂Flu, I*)ZrCl₂ (2_{sMAO}): ¹³C CP/MAS NMR (10 kHz, 298 K) δ (ppm): 137.0, 128.2, 119.8, 35.2, 30.3, 15.9 and -8.1. ²⁹Si CP/MAS NMR (10 kHz, 298 K) δ (ppm): -5.3 and -20.6. ²⁷Al DP/MAS NMR (15 kHz, 298 K) δ (ppm): 343.8, 203.3, 68.2, -83.0 and -240.0.

sMAO-Me²SB(Cp, I*)Zr(CH₂SiMe₃)₂ (3_{sMAO}): ¹³C CP/MAS NMR (10 kHz, 298 K) δ (ppm): 136.6, 129.5, 52.3, 17.2 and -7.8. ²⁹Si CP/MAS NMR (10 kHz, 298 K) δ (ppm): 0.6 and -11.8. ²⁷Al DP/MAS NMR (15 kHz, 298 K) δ (ppm): 313.4, 164.4, -92.7 and -252.2.

LDHMAO-Me²SB(Cp, I*)Zr(CH₂SiMe₃)₂ (3_{LDHMAO}): ¹³C CP/MAS NMR (10 kHz, 298 K) δ (ppm): 166.7, 131.2, 66.4, 55.3, 17.2 and -7.8. ²⁹Si CP/MAS NMR (10 kHz, 298 K) δ (ppm): 0.8 and -13.6. ²⁷Al DP/MAS NMR (15 kHz, 298 K) δ (ppm): 451.7, 318.4, 117.1, 18.5 and -244.4.

5.11 Slurry-phase ethylene polymerisation

Scavenger ([Al_{scav}]₀/[Zr]₀ = 1000) in hexane (10 mL) was added to a 150 mL Rotaflo ampoule. The supported complex (10 mg) was added and washed with hexane (40 mL). The ampoule headspace was degassed whilst heating to temperature. The ampoule was opened to ethylene gas (2 bar) and the solution stirred at 1000 rpm for the duration of the run. On completion, the reaction mixture was degassed and the polymer filtered, washed with pentane (2 × 25 mL) and dried under reduced pressure on a frit. All runs were carried out, at least, in duplicate.

Acknowledgments

J. V. L., J.-C. B. and Z. R. T. (SCG Research Fellowship) would like to thank SCG Chemicals Co., Ltd. (Thailand) for financial support; Dr Nicholas H. Rees (University of Oxford) for solid-state NMR spectroscopy experiments; Chemical Crystallography (University of Oxford) for the use of the diffractometers; Research Complex at Harwell for use of the Scanning Electron Microscope; Ms Liv Thobru (Norner AS, Norway) for GPC, and Prof. Charlotte Williams (University of Oxford) for use of the Differential Scanning Calorimeter.

References

1. L. Resconi, L. Cavallo, A. Fait and F. Piemontesi, *Chem. Rev.*, 2000, **100**, 1253-1346.
2. G. G. Hlatky, *Chem. Rev.*, 2000, **100**, 1347-1376.

3. W. Kaminsky, A. Funck and H. Haehnsen, *Dalton Trans.*, 2009, 8803-8810.
4. I. Sedov, V. Makhaev and P. E. Matkovskii, *Catal. Ind.*, 2012, **4**, 129-140.
5. P. J. Shapiro, *Coord. Chem. Rev.*, 2002, **231**, 67-81.
6. B. Wang, *Coord. Chem. Rev.*, 2006, **250**, 242-258.
7. J.-C. Buffet, Z. R. Turner and D. O'Hare, *Chem. Commun.*, 2018, **54**, 10970-10973.
8. P. Ransom, A. E. Ashley, N. D. Brown, A. L. Thompson and D. O'Hare, *Organometallics*, 2011, **30**, 800-814.
9. J.-C. Buffet, T. A. Q. Arnold, Z. R. Turner, P. Angpanitcharoen and D. O'Hare, *RSC Adv.*, 2015, **5**, 87456-87464.
10. H. G. Alt and A. Koppl, *Chem. Rev.*, 2000, **100**, 1205-1221.
11. G. Tian, B. Wang, S. Xu, Y. Zhang and X. Zhou, *J. Organomet. Chem.*, 1999, **579**, 24-29.
12. C. Copéret and J.-M. Basset, *Adv. Synth. Catal.*, 2007, **349**, 78-92.
13. C. Copéret, F. Allouche, K. W. Chan, M. P. Conley, M. F. Delley, A. Fedorov, I. B. Moroz, V. Mougel, M. Pucino, K. Searles, K. Yamamoto and P. A. Zhizhko, *Angew. Chem., Int. Ed.*, 2018, **57**, 6398-6440.
14. J. D. A. Pelletier and J.-M. Basset, *Acc. Chem. Res.*, 2016, **49**, 664-677.
15. C. Copéret, A. Fedorov and P. A. Zhizhko, *Catal. Lett.*, 2017, **147**, 2247-2259.
16. C. Copéret, A. Comas-Vives, M. P. Conley, D. P. Estes, A. Fedorov, V. Mougel, H. Nagae, F. Nunez-Zarur and P. A. Zhizhko, *Chem. Rev.*, 2016, **116**, 323-421.
17. C. Copéret, M. Chabanas, R. P. Saint-Arroman and J.-M. Basset, *Angew. Chem., Int. Ed.*, 2003, **42**, 156-181.
18. R. Anwender, *Chem. Mater.*, 2001, **13**, 4419-4438.
19. P. Serna and B. C. Gates, *Acc. Chem. Res.*, 2014, **47**, 2612-2620.
20. M. K. Samantaray, E. Pump, A. Bendjeriou-Sedjerari, V. D'Elia, J. D. A. Pelletier, M. Guidotti, R. Psaro and J.-M. Basset, *Chem. Soc. Rev.*, 2018, **47**, 8403-8437.
21. J. A. Ewen, *J. Am. Chem. Soc.*, 1984, **106**, 6355-6364.
22. J. A. Ewen, R. L. Jones, A. Razavi and J. D. Ferrara, *J. Am. Chem. Soc.*, 1988, **110**, 6255-6256.
23. V. F. Tisse, F. Prades, R. Briquel, C. Boisson and T. F. L. McKenna, *Macromol. Chem. Phys.*, 2010, **211**, 91-102.
24. A. Entezami and P. N. Moghadam, *Polym. Int.*, 2005, **54**, 1326-1329.
25. J. R. Severn, J. C. Chadwick, R. Duchateau and N. Friederichs, *Chem. Rev.*, 2005, **105**, 4073-4147.
26. K. Soga and M. Kaminaka, *Macromol. Chem. Phys.*, 1993, **194**, 1745-1755.
27. S. Collins, W. M. Kelly and D. A. Holden, *Macromolecules*, 1992, **25**, 1780-1785.
28. M. M. Stalzer, M. Delferro and T. J. Marks, *Catal. Lett.*, 2015, **145**, 3-14.
29. C. P. Nicholas, H. Ahn and T. J. Marks, *J. Am. Chem. Soc.*, 2003, **125**, 4325-4331.
30. M. P. McDaniel, M. D. Jensen, K. Jayaratne, K. S. Collins, E. A. Benham, N. D. McDaniel, P. K. Das, J. L. Martin, Q. Yang, M. G. Thorn and A. P. Masino, in *Tailor-Made Polymers*, eds. J. R.

- Severn and J. C. Chadwick, Wiley-VCH, Verlag GmbH & Co. KGaA, Weinheim, 2008, pp. 171-210.
31. T. A. Q. Arnold, Z. R. Turner, J.-C. Buffet and D. O'Hare, *J. Organomet. Chem.*, 2016, **822**, 85-90.
 32. D. A. X. Fraser, Z. R. Turner, J.-C. Buffet and D. O'Hare, *Organometallics*, 2016, **35**, 2664-2674.
 33. T. J. Williams, J.-C. Buffet, Z. R. Turner and D. O'Hare, *Catal. Sci. Technol.*, 2018, **8**, 5454-5461.
 34. I. I. Zakharov, V. A. Zakharov, A. G. Potapov and G. M. Zhidomirov, *Macromol. Theory Simul.*, 1999, **8**, 272-278.
 35. J. V. Lamb, J.-C. Buffet, Z. R. Turner and D. O'Hare, *Polym. Chem.*, 2019, **10**, 1386-1398.
 36. J. V. Lamb, J.-C. Buffet, J. E. Matley, C. M. R. Wright, Z. R. Turner and D. O'Hare, *Dalton Trans.*, 2019, **48**, 2510-2520.
 37. S. Gutmann, P. Burger, H.-U. Hund, J. Hofmann and H.-H. Brintzinger, *J. Organomet. Chem.*, 1989, **369**, 343-357.
 38. O. Perez-Camacho, S. Y. Knjazhanski, G. Cadenas, M. J. Rosales-Hoz and M. A. Leyva, *J. Organomet. Chem.*, 1999, **585**, 18-25.
 39. A. V. Firth, J. C. Stewart, A. J. Hoskin and D. W. Douglas, *J. Organomet. Chem.*, 1999, **591**, 185-193.
 40. W. A. Howard, T. M. Trnka and G. Parkin, *Inorg. Chem.*, 1995, **34**, 5900-5909.
 41. N. Senso, S. Khaubunsongserm, B. Jongsomjit and P. Praserttham, *Molecules*, 2010, **15**, 9323-9339.
 42. H. Hammawa, T. M. Mannan, D. T. Lynch and S. E. Wanke, *J. Appl. Polym. Sci.*, 2004, **92**, 3549-3560.
 43. D. T. Lynch, M. O. Jejelowo and S. E. Wanke, *Can. J. Chem. Eng.*, 1991, **69**, 657-664.
 44. N. V. Semikolenova and V. A. Zakharov, 1997, **198**, 2889-2897.
 45. J. T. Hirvi, M. Bochmann, J. R. Severn and M. Linnolahti, *ChemPhysChem*, 2014, **15**, 2732-2742.
 46. F. Q. Song, R. D. Cannon and M. Bochmann, *J. Am. Chem. Soc.*, 2003, **125**, 7641-7653.
 47. M. Bochmann and S. J. Lancaster, *Angew. Chem., Int. Ed.*, 1994, **33**, 1634-1637.
 48. V. F. Tisse, C. Boisson and T. F. L. McKenna, *Macromol. Chem. Phys.*, 2014, **215**, 1358-1369.
 49. W. Michiels and A. Munozescalona, *Macromol. Symp.*, 1995, **97**, 171-183.
 50. J. E. O'Hara and K. B. Wagener, *Makromol. Chem., Rapid Commun.*, 1993, **14**, 657-662.
 51. G. Rojas, B. Inci, Y. Wei and K. B. Wagener, *J. Am. Chem. Soc.*, 2009, **131**, 17376-17386.
 52. A. S. Vaughan and D. C. Bassett, in *Comprehensive Polymer Science and Supplements*, eds. G. Allen and J. C. Bevington, Pergamon, Amsterdam, 1989, pp. 415-457.
 53. C. F. Luo, M. Kroger and J. U. Sommer, *Polymer*, 2017, **109**, 71-84.
 54. C. B. Crawford and B. Quinn, in *Microplastic Pollutants*, eds. C. B. Crawford and B. Quinn, Elsevier, 2017, pp. 57-100.
 55. T. Repo, G. Jany, M. Salo, M. Polamo and M. Leskela, *J. Organomet. Chem.*, 1997, **541**, 363-366.
 56. C. M. R. Wright, Z. R. Turner, J.-C. Buffet and D. O'Hare, *Chem. Commun.*, 2016, **52**, 2850-2853.

57. A. Macchioni, *Chem. Rev.*, 2005, **105**, 2039-2074.
58. E. Zurek and T. Ziegler, *Organometallics*, 2002, **21**, 83-92.
59. E. Zurek and T. Ziegler, *Prog. Polym. Sci.*, 2004, **29**, 107-148.
60. M. A. Parvez, M. Rahaman, M. A. Suleiman, J. B. P. Soares and I. A. Hussein, *Int. J. Polym. Sci.*, 2014, 1-10.
61. L. D 'Agnillo, J. B. P. Soares and A. Penlidis, *Macromol. Chem. Phys.*, 1998, **199**, 955-962.
62. M. D. F. V. Marques and R. B. Tiosso, *J. Mater. Sci. Eng. Adv. Tech.*, 2011, **4**, 149-173.
63. J.-C. Buffet, N. Wana, T. A. Q. Arnold, E. K. Gibson, P. P. Wells, Q. Wang, J. Tantirungrotechai and D. O'Hare, *Chem. Mater.*, 2015, **27**, 1495-1501.
64. J.-C. Buffet, Z. R. Turner, R. T. Cooper and D. O'Hare, *Polym. Chem.*, 2015, **6**, 2493-2503.
65. C. Chen, M. Yang, Q. Wang, J.-C. Buffet and D. O'Hare, *J. Mater. Chem. A.*, 2014, **2**, 15102-15110.
66. Q. Wang and D. O'Hare, *Chem. Commun.*, 2013, **49**, 6301-6303.